JOURNAL OF NEUROPHYSIOLOGY
Vol. 69, No. 4, April 1993. *Printed in U.S.A.*

Spatiotemporal Organization of Simple-Cell Receptive Fields in the Cat's Striate Cortex. I. General Characteristics and Postnatal Development

G. C. DEANGELIS, I. OHZAWA, AND R. D. FREEMAN
Groups in Bioengineering and Neurobiology, and School of Optometry, University of California, Berkeley, California 94720

SUMMARY AND CONCLUSIONS

1. Most studies of cortical neurons have focused on the spatial structure of receptive fields. For a more complete functional description of these neurons, it is necessary to consider receptive-field structure in the joint domain of space and time. We have studied the spatiotemporal receptive-field structure of 233 simple cells recorded from the striate cortex of adult cats and kittens at 4 and 8 wk postnatal. The dual goal of this study is to provide a detailed quantitative description of spatiotemporal receptive-field structure and to compare the developmental time courses of spatial and temporal response properties.

2. Spatiotemporal receptive-field profiles have been measured with the use of a reverse correlation method, in which we compute the cross-correlation between a neuron's response and a random sequence of small, briefly presented bright and dark stimuli. The receptive-field profiles of some simple cells are space-time *separable,* meaning that spatial and temporal response characteristics can be dissociated. Other cells have receptive-field profiles that are space-time *inseparable.* In these cases, a particular spatial location cannot be designated, unambiguously, as belonging to either an ON or OFF subregion. However, separate ON and OFF subregions may be clearly distinguished in the joint space-time domain. These subregions are generally tilted along an oblique axis.

3. Our observations show that spatial and temporal aspects of receptive-field structure mature with clearly different time courses. By 4 wk postnatal, the spatial symmetry and periodicity of simple-cell receptive fields have reached maturity. The spatial extent (or size) of these receptive fields is adultlike by 8 wk postnatal. In contrast, the response latency and time duration of spatiotemporal receptive fields do not mature until well beyond 8 wk postnatal.

4. By applying Fourier analysis to spatiotemporal receptive-field profiles, we have examined the postnatal development of spatial and temporal selectivity in the frequency domain. By 8 wk postnatal, spatial frequency tuning has clearly reached maturity. On the contrary, temporal frequency selectivity remains markedly immature at 8 wk. We have also examined the joint distribution of optimal spatial and temporal frequencies. From 4 wk postnatal until 8 wk postnatal, the range of optimal spatial frequencies increases substantially, whereas the range of optimal temporal frequencies remains largely unchanged. From 8 wk postnatal until adulthood, there is a large increase in optimal temporal frequencies for cells tuned to low spatial frequencies. For cells tuned to high spatial frequencies, the distribution of optimal temporal frequencies does not change much beyond 8 wk postnatal.

5. By summing the frequency spectra of all simple cells within a particular age group, we have constructed a population frequency response. Predictions of spatial and temporal contrast sensitivity based on the population response agree reasonably well with behavioral measurements of contrast sensitivity.

6. From spatiotemporal receptive-field profiles, we have also obtained estimates of velocity preference and direction selectivity for simple cells. There is little difference in these parameters between populations of simple cells from adult cats and kittens.

7. Overall, our findings show that most simple-cell receptive fields cannot be adequately described by a single spatial sensitivity profile. Valuable insights are gained by examining these receptive fields in the joint domain of space and time.

INTRODUCTION

Unlike cells at earlier stages in the visual pathway, neurons in the primary visual cortex are finely tuned to stimulus parameters such as orientation, spatial frequency, and direction of motion (Cooper and Robson 1968; Hubel and Wiesel 1962; Maffei and Fiorentini 1973; for review see Orban 1991). Since the original description of the receptive fields of visual cortical cells (Hubel and Wiesel 1959, 1962), many researchers have studied the development of neuronal response properties during early postnatal life (for reviews, see Fregnac and Imbert 1984; Mitchell and Timney 1984; Movshon and Van Sluyters 1981). Kittens reared in a normal environment have been used extensively as an animal model in this work. Previous studies have focused mainly on the development of orientation selectivity (Albus and Wolf 1984; Blakemore and Van Sluyters 1975; Bonds 1979; Braastad and Heggelund 1985; Buisseret and Imbert 1976; Fregnac and Imbert 1978; Hubel and Wiesel 1963; Pettigrew 1974; Sherk and Stryker 1976), spatial frequency selectivity (Derrington and Fuchs 1981), and the spatial structure of receptive fields (Albus and Wolf 1984; Blakemore and Van Sluyters 1975; Braastad and Heggelund 1985; Buisseret and Imbert 1976; Fregnac and Imbert 1978; Hubel and Wiesel 1963). The central question addressed in these studies is whether the receptive-field characteristics and stimulus selectivities of single neurons are determined innately or require visual experience to develop. Although the findings are somewhat conflicting (see Barlow and Pettigrew 1971 and Hubel and Wiesel 1963, for example), the general consensus is that normal response properties can be observed at the time of eye opening but require several weeks of visual experience to reach adult levels of specificity.

Although the spatial structure of receptive fields has received a great deal of attention, relatively little is known about changes in temporal receptive-field characteristics

during normal postnatal development. It is of interest to know whether spatial and temporal response properties mature with similar or different time courses. Moreover, it is important to establish whether spatial and temporal processes of development are interrelated (e.g., whether development of temporal frequency selectivity depends on spatial frequency, and vice versa). To address these questions, it is necessary to examine both spatial and temporal receptive-field characteristics. Apparently, neither the temporal structure of receptive fields nor the temporal frequency tuning of single cells in the striate cortex has been studied developmentally in kittens. In fact, temporal aspects of receptive-field structure have not been studied extensively even in adult cats. The study we report here, which has two primary goals, is intended to fill these gaps. First, we provide a comprehensive description of the spatiotemporal receptive-field structure of simple cells in the cat's striate cortex. Second, we examine how temporal aspects of receptive-field structure mature during normal postnatal development. With regard to the latter point, we compare the developmental time course of changes in temporal receptive-field properties with that of spatial properties.

To measure the spatiotemporal structure of receptive fields, we have used a version of the reverse correlation algorithm (DeBoer and Kuyper 1968; Eggermont et al. 1983; Sutter 1975) for mapping receptive fields. Jones and Palmer (1987a) have shown that this technique provides detailed two-dimensional spatial receptive-field profiles for simple cells in adult cats. In addition, we have recently used this method to study the receptive-field structure and disparity selectivity of binocular cells (DeAngelis et al. 1991; Freeman and Ohzawa 1990; Ohzawa et al. 1990). As described previously (McLean and Palmer 1989; Palmer et al. 1991), the reverse correlation algorithm can be extended to produce receptive-field profiles as a function of both space and time. This method is advantageous for developmental studies because it provides a highly quantitative description of receptive-field structure, whereas previous studies have often relied on hand plotting of receptive fields or subjective classification of response properties (see Mitchell and Timney 1984). Another advantage is that we can apply Fourier analysis to the spatiotemporal receptive-field profiles of simple cells to obtain estimates of spatial and temporal frequency tuning. Of course, this approach requires that cells exhibit linear spatial and temporal summation, which is clearly not the case for complex cells (e.g., Movshon et al. 1978b). As a result, the scope of this study is limited to simple cells. The companion paper (DeAngelis et al. 1993) addresses the issue of linearity in detail and establishes the validity of the approach used here.

We have applied the reverse correlation algorithm to map the spatiotemporal receptive fields of simple cells from kittens at 4 and 8 wk postnatal and from adult cats. In addition, we have applied Fourier analysis to obtain measurements of the spatial and temporal frequency selectivity of these neurons, as well as estimates of their velocity and direction selectivity. Our results demonstrate that the temporal structure of simple-cell receptive fields, like the spatial structure, matures gradually over the first several weeks of postnatal life. There is a clear difference, however, between the developmental time course for spatial and temporal receptive-field characteristics. At 8 wk postnatal, the spatial properties of simple-cell receptive fields are indistinguishable from those in adult cats, whereas temporal receptive-field characteristics are still markedly immature. Our findings also demonstrate that spatial and temporal processes of development are not independent. From 8 wk postnatal until adulthood, there is a pronounced increase in temporal resolution for neurons tuned to low spatial frequencies, with little change in temporal selectivity for neurons preferring high spatial frequencies.

METHODS

All experiments were performed with cats reared in a normal environment. Kittens at 4 wk postnatal ranged in weight between 0.35 and 0.6 kg, and kittens at 8 wk of age weighed between 0.56 and 0.91 kg. Adult cats ranged in weight from 1.9 to 5.1 kg.

Surgical procedures

After initial preanesthetic doses of acepromazine (0.5 mg/kg sc) and atropine (0.3 mg sc for adult cats, 0.05 mg sc for kittens), each cat is anesthetized with halothane (2.5–3% in O_2) for the remainder of the surgical preparation. A rectal temperature probe is inserted, electrocardiographic (ECG) electrodes are secured, and a femoral vein is catheterized. Subsequently, a tracheostomy is performed and a tracheal tube inserted. The animal is then secured in a stereotaxic apparatus with the use of ear bars. Electroencephalographic (EEG) screw electrodes are placed over the frontal sinus, and a section of skull and dura (~5 mm diam) are removed to allow insertion of a pair of tungsten-in-glass electrodes (Levick 1972). Two electrodes are used to increase the chance of encountering cells and to obtain simultaneous recordings from two or more cells, as described in other studies (DeAngelis et al. 1992; Ghose et al. 1990, 1991). For adults, the craniotomy is centered at Horsley-Clarke coordinates P4 L2. For 4-wk-old kittens, the craniotomy is centered ~2–3 mm anterior and 1–2 mm lateral to the lambda suture, which is a prominent landmark on the skull over the occipital lobe. For 8-wk-old kittens, the craniotomy is centered halfway between the location determined by the Horsley-Clarke coordinates and that specified by the lambda suture. After lowering the electrodes to the cortical surface, agar is used to insulate the cortex, and melted wax is applied over the agar to create a sealed chamber. The cat is then paralyzed with gallamine triethiodide (Flaxedil), which is continuously infused at a rate of 10 $mg \cdot kg^{-1} \cdot h^{-1}$, along with 1 $mg \cdot kg^{-1} \cdot h^{-1}$ of sodium thiamylal (Surital) as an anesthetic supplement. Artificial ventilation is carried out with a gas mixture of 70% N_2O-29% O_2-1% CO_2. The respirator is set at 25 strokes/min, and stroke volume is adjusted to maintain a constant end-tidal CO_2 of ~4.5%. Body temperature is maintained near 38°C with the use of a servo-controlled heating pad. Heart rate, EEG, ECG, and intratracheal pressure are monitored continuously. Pupils are dilated with atropine (1%) and nictitating membranes are retracted with 10% phenylephrine hydrochloride (Neo-Synephrine). Contact lenses (+2.0 D) with 4-mm artificial pupils are then positioned on each cornea. For additional details, see Freeman and Ohzawa (1988) and Ohzawa and Freeman (1986).

At the end of an experiment, the animal is administered an overdose of pentobarbital sodium (Nembutal). After perfusion and fixation (with a buffered 0.9% saline solution followed by 10% Formalin), the cortex is frozen and sectioned into 40-μm slices. Tissue is stained with thionin, electrode tracks are reconstructed, and laminae identified. Histological analysis confirmed that all cells were recorded from area 17.

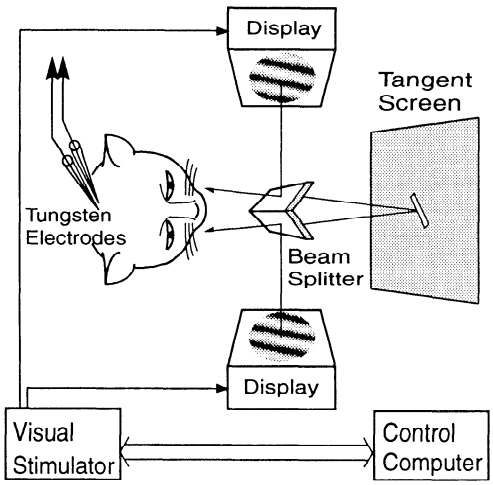

FIG. 1. Schematic diagram of the experimental apparatus used in this study. See text for details.

Experimental apparatus

The apparatus used for conducting these experiments is shown schematically in Fig. 1. The cat is positioned in a stereotaxic apparatus, with head position fixed by means of ear bars and a mouth bar. The animal faces a large rear-projection screen, at a distance of 57 cm, on which variable dimension bars of light can be swept manually via a joystick. A pair of beam splitters (70% reflectance) is placed in front of the cat's eyes, with each beam splitter oriented diagonally at ~45° to the optical axes of the eyes. The beam splitters allow the cat to view stimuli on the tangent screen, as well as patterns that are presented on either of two video displays, one for each eye. The video displays (Mitsubishi Electronics; mean luminance, 45 cd/m^2; screen size, 28 × 22 cm) have a resolution of 1,024 × 804 pixels and are refreshed at 76 Hz. Visual stimuli are generated on these displays by a dedicated computer that employs two high-resolution graphics boards (Imagraph). This visual stimulator is capable of generating sinusoidal grating stimuli of arbitrary size, spatial frequency, orientation, velocity, and contrast. In addition, bright and dark bars of variable size and orientation can be presented at any position on the screen. A second computer controls the visual stimulator through a serial port and coordinates data acquisition, real-time analysis, and data display.

The tungsten-in-glass microelectrodes are advanced through the cortex by a piezo-electric micropositioner (Burleigh). The signals from each electrode are then amplified, band-pass filtered (100–10,000 Hz), and fed into a two-channel window discriminator. On the basis of amplitude discrimination with the use of a pair of reference levels, the window discriminator signals the occurrence of each selected action potential as a logic pulse. The time of occurrence and input channel of each pulse event is then recorded with 1-ms resolution and stored on disk. These signals are also used by the controlling computer to generate response histograms, which are displayed in real time on a high-resolution color monitor.

Preliminary procedures

The optic disks are projected onto the large tangent screen with the use of a reversible ophthalmoscope. The positions of the areae centrales are then estimated from the positions of the optic disks. Once the action potential of a single cell is isolated, the receptive field is initially explored with a bar of light that is moved manually. The location of the receptive field is marked on plotting paper by means of a large beam splitter behind the rear-projection screen. Ocular dominance is also estimated at this time.

Before starting quantitative measurements, preliminary observations are made to determine each cell's preferred orientation and spatial frequency, as well as the size of its receptive field. Whether or not the cell exhibits end or side inhibition is also evaluated. This is done with the use of a "search" program, in which the orientation, spatial frequency, position, and size of a patch of drifting sinusoidal grating can be controlled with the use of a pointing device. By adjusting the parameters of the stimulus and observing the response, one can obtain a good estimate of a cell's preferred orientation and spatial frequency. By adjusting the location of a small patch of grating to give the largest response, the center position of the receptive field can be located quite accurately.

Having completed this search procedure, quantitative measurements of the cell's orientation and spatial frequency tuning are obtained by presenting sequences of drifting sinusoidal gratings, in which one of these parameters is varied. In some of these experiments, temporal frequency tuning curves have also been obtained. Typically, large field (10–20° diam) grating stimuli are used for these tests, unless the cell exhibits end or side inhibition in the preliminary observations. When this is observed, the grating stimuli are adjusted to be of optimal size for the cell (DeAngelis et al. 1990). To construct tuning curves, gratings are presented for 4 s each in blocks of randomly interleaved trials, during which peristimulus time histograms (PSTHs) of the responses are accumulated. Each stimulus is typically presented four to six times, and successive stimuli are separated by a period of 2–3 s during which the animal views blank screens of the same mean luminance as the gratings. For binocular cells, tuning curves are constructed for each eye by interleaving left and right eye stimuli during this process. After presentation of the complete set of stimuli, the magnitude of the accumulated response to each different stimulus is evaluated by Fourier analysis of the PSTHs. The mean firing rate, as well as the first and second harmonics of the response, are computed. Because the responses of simple cells to drifting sinusoidal gratings are modulated at the temporal frequency of the stimulus, the ratio of the amplitude of the first harmonic to the mean firing rate can be used to classify simple cells (see Skottun et al. 1991 for review).

Reverse correlation analysis

To measure spatiotemporal receptive-field profiles for cortical cells, we have used a reverse correlation technique (DeBoer and Kuyper 1968; Eggermont et al. 1983; Sutter 1975), which is very similar to that described by Jones and Palmer (1987a) and Palmer et al. (1991). The basic goal is to obtain an estimate of the spatiotemporal *impulse response* of a single cortical neuron. Traditionally, this type of measurement is obtained by repeatedly presenting a brief stimulus and recording the response of the neuron over some period of time after the stimulus. An alternate approach is to stimulate the neuron with a continuous, random sequence of very brief stimuli and to store the ongoing response of the neuron. By cross-correlating the response of the neuron with the stimulus sequence, one can obtain an input-output relationship for the neuron (see also Palmer et al. 1991). If the stimulus sequence approximates white noise and the neuron behaves linearly, this cross-correlation procedure yields the spatiotemporal impulse response of the neuron (see DeBoer and Kuyper 1968). The advantage of this method for studying cortical neurons is that a highly detailed spatiotemporal receptive-field profile can be obtained in a fraction of the time required with the use of the traditional approach described above. The assumption that our stimulus approximates white noise is examined in the APPENDIX; the assumption of linearity is examined in the companion paper (DeAngelis et al. 1993).

An efficient algorithm for computing the cross-correlation between stimulus and response is known as *reverse correlation*, or triggered correlation (DeBoer and Kuyper 1968). Our reverse

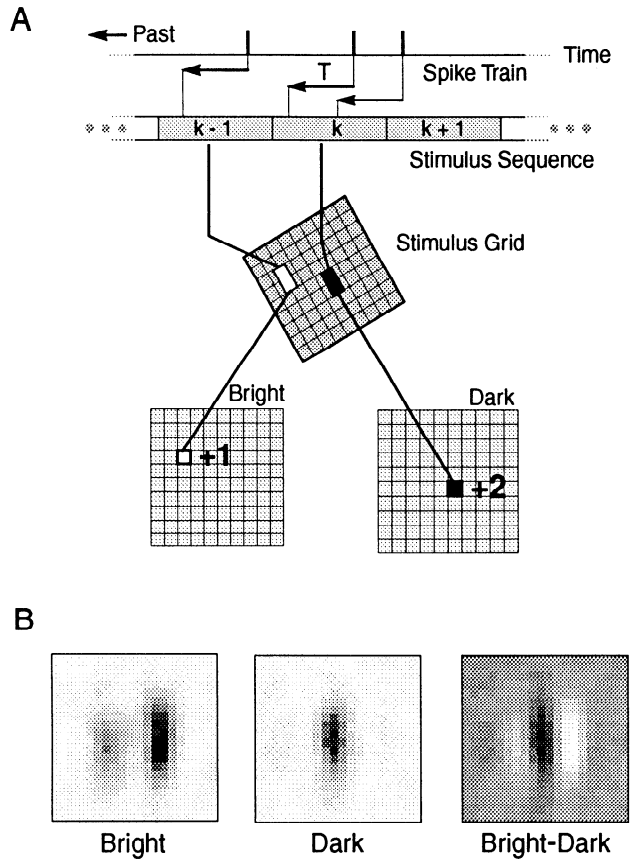

FIG. 2. *A*: schematic illustration of the reverse correlation algorithm for mapping receptive fields. The stimulus is a sequence (denoted $\cdots k-1, k, k+1 \cdots$) of small bright and dark rectangular bars. These bars are presented, in random order, on a stimulus grid (shown in the center of the figure) that is oriented to match the preferred orientation of the neuron being studied. The train of action potentials produced by the neuron is shown at the *top*, in temporal register with the stimulus sequence. Each action potential is assigned to the stimulus that precedes it by a delay of T ms (see arrows pointing to the left). For example, the leftmost action potential in the spike train is assigned to the $(k-1)$th stimulus, which is a bright bar located near the top left corner of the stimulus grid. To record this event, we update the 2-dimensional (2-D) histogram labeled "Bright" by adding +1 to the bin corresponding to the location of the stimulus on the grid. Similarly, the next 2 spikes in the train are assigned to the kth stimulus (a dark bar), and the histogram labeled "Dark" is updated. See text for additional details. *B*: 2-D spatial receptive-field profile for a simple cell, obtained by the use of the reverse correlation technique. Each square panel represents an area of visual space (in this case, $5 \times 5°$), which is slightly larger than the cell's receptive field. *Left*: 2-D spatial profile obtained in response to a bright bar stimulus. *Middle*: 2-D profile obtained in response to a dark bar. The darker a point in each of these panels, the more likely the cell is to respond to a bar stimulus centered at that location. Note that the responses elicited by bright and dark bars form spatially segregated, elongated subregions. This is characteristic of a simple cell. *Right*: composite receptive-field profile obtained by taking the difference of the bright and dark bar responses. In this composite profile, the lightest spots represent strong responses to a bright bar, and the darkest spots are indicative of strong response to a dark bar. Areas in which neither a bright or dark stimulus causes the cell to respond are shaded grey.

correlation algorithm is diagramed in Fig. 2*A* (see also Freeman and Ohzawa 1990; Jones and Palmer 1987a; Palmer et al. 1991). The visual stimulus is a pseudorandom sequence of small bright and dark rectangular bars that are presented on a stimulus grid that typically has 20×20 locations. This stimulus grid is positioned such that its center corresponds to the center position of the receptive field, as determined in the search procedure described above. In addition, the size of the stimulus grid is adjusted so that it covers the entire receptive field. Both the stimulus grid and the small bar stimuli are oriented to match the cell's preferred orientation. Each bar stimulus is centered at one of the 20×20 locations on the stimulus grid. The bar stimuli are typically $\sim 1.5 \times 0.5°$ in size and are presented for a duration of 40 ms, although these parameters are varied somewhat from cell to cell. In general, there is a trade-off between resolution and stimulus energy. Ideally, one would like to use stimuli that are very small and presented for very short durations, to maximize spatial and temporal resolution and to satisfy the assumption that each stimulus approximates an impulse (see APPENDIX). However, most cells will not respond to such stimuli because they have very little energy. Thus we generally attempt to make the stimuli as small as possible, in both space and time, such that they still elicit a reasonable response from the neuron. In practice, these choices are guided by the spatial and temporal frequency tuning curves obtained with the use of gratings. For cells that respond to high spatial frequencies, small stimuli must be used such that the spatial resolution of the reverse correlation technique is higher than the spatial resolution of the cell's receptive field. Similar considerations apply to the choice of stimulus duration, which can be guided by the measured temporal frequency tuning.

The reverse correlation algorithm operates as follows (see Fig. 2*A*). Individual bar stimuli are presented one at a time, in rapid succession, on the stimulus grid. For each successive 40-ms presentation, both the location of the bar on the stimulus grid and the contrast of the bar (bright or dark) are chosen randomly. Each time an action potential occurs, we assign it to the stimulus that preceded it by a delay period of T milliseconds. During the data collection, we assume a particular value of T. Previous studies (DeAngelis et al. 1991; Jones and Palmer 1987a) have shown that values ranging from 50 to 80 ms are quite effective for most cells. After the data have been collected, we analyze over a range of values of T (see below). Once a spike has been assigned to its likely causal stimulus (i.e., the one that precedes it by T ms), we increment a two-dimensional (2-D) histogram bin at the coordinate that corresponds to the location of the causal stimulus on the stimulus grid. Separate histograms are collected for the responses to bright and dark bars. This assignment process is repeated for each action potential that is elicited by the stimulus sequence. For a stimulus grid having 20×20 locations, one stimulus sequence consists of 800 different bar stimuli (400 grid locations times 2 bar contrasts), and lasts ~ 32 s (if we assume that each bar is presented for 40 ms). Each bar stimulus occurs once and only once during each stimulus sequence. Usually, the stimulus sequence is repeated 20–50 times to obtain enough spikes (on the order of a few thousand) for a smooth receptive-field profile. Thus the time required for a complete measurement of the receptive-field profile is in the range of 10–25 min. Note that the presentation order of stimuli is rerandomized each time the stimulus sequence is repeated, such that a particular temporal sequence of bright and dark bars is never repeated.

Figure 2*B* shows a typical receptive-field profile for a simple cell, as obtained by reverse correlation. The *left* and *middle panels* show, as two-dimensional density plots, the response profiles for bright and dark stimuli, respectively. A composite receptive-field profile is obtained by taking the difference of the bright and dark bar responses, as shown in the *right panel* of Fig. 2*B*. The assumptions underlying this subtraction operation are addressed in the DISCUSSION. In the composite profile, regions responsive to bright stimuli are shown in shades of gray approaching white, whereas regions responding to dark stimuli are shaded nearly black. This composite profile gives the 2-D spatial structure of the receptive field for one particular value ($T = 60$ ms) of the reverse correlation delay, T.

A major focus of this study is to describe how the spatial struc-

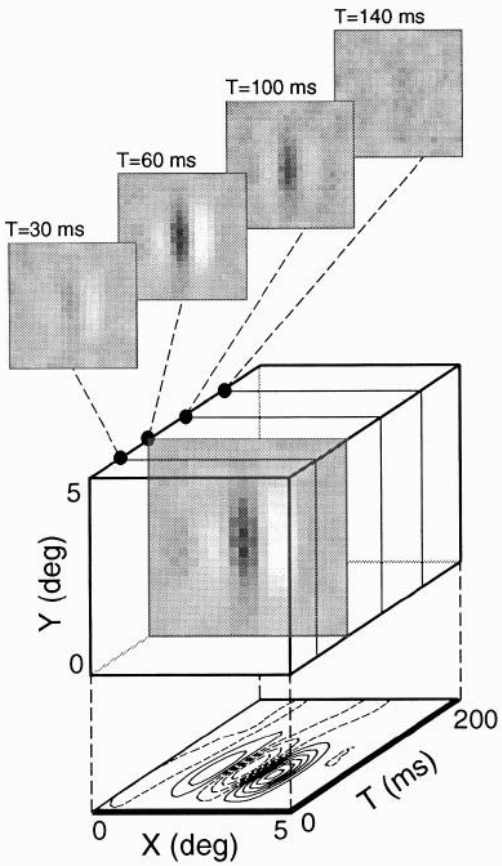

FIG. 3. Method of constructing spatiotemporal receptive-field profiles for simple cells. The 4 stacked panels (*top*) show the 2-dimensional (2-D) spatial receptive-field profile (for the same simple cell shown in Fig. 2*B*) for 4 different values of the reverse correlation delay parameter (T = 30, 60, 100, 140 ms). Each 2-D spatial profile is shown as a grey-scale density plot, where "white" pixels indicate response to a small bright bar and "black" pixels indicate response to a small dark bar. Computing the 2-D spatial receptive-field profile for many different values of T yields the 3-dimensional (3-D) data set shown as a cube, where X and Y correspond to the 2 spatial dimensions of the reverse correlation stimulus grid, and T is the reverse correlation delay. Slicing through this cube at any value of T yields a corresponding 2-D spatial receptive-field profile (the T = 60 ms profile is shown within the cube as an example). Integrating this 3-D data set along the Y-axis (i.e., parallel to the cell's preferred orientation) yields a simplified spatiotemporal receptive-field profile, or X-T plot (McLean and Palmer 1989), which is shown below the cube as a contour map. This X-T plot shows the cell's 1-D spatial sensitivity profile (along the X dimension) as a function of the time delay, T, between stimulus onset and elicited spike activity. Solid contour lines represent bright-excitatory (or ON) receptive-field subregions; dashed contours represent dark-excitatory (or OFF) receptive-field subregions.

ture of simple-cell receptive fields changes with time, in both cats and kittens. For this purpose, the reverse correlation algorithm can be extended to produce a spatiotemporal receptive-field profile (McLean and Palmer 1989; Palmer et al. 1991). This process is illustrated in Fig. 3. The complete spatiotemporal receptive-field profile, illustrated by the cube in Fig. 3, is a function of three independent variables: X, Y, and T. X and Y are the two spatial dimensions of the receptive field, and T is time. By convention, Y is always the dimension of the receptive field that is parallel to the cell's preferred orientation. Hence X is the dimension that cuts across the elongated bright- and dark-excitatory subregions, as usually displayed in a line-weighting function (e.g., DeValois et al. 1978; Movshon et al. 1978a). Because it is difficult to display the full spatiotemporal receptive-field profile, we integrate along Y to obtain a simplified description, which we shall call an X-T plot. This is shown at the *bottom* of Fig. 3 as an isoamplitude contour map.

Throughout this paper, X-T profiles will be displayed as contour plots; hence a brief description of the construction of these plots is necessary. Each X-T profile typically has a resolution of 20 points in space (X) and 20 points in time (T). The data are smoothed with the use of a very small Gaussian filter, which removes high-frequency (i.e., spurious) noise in the data. The parameters of this filter are chosen such that its roll-off does *not* substantially attenuate frequencies within the spatiotemporal pass band of a given neuron. Once smoothed, the X-T data are interpolated and plotted as a contour map. Contours are drawn at amplitudes which are ±10, 30, 50, 70, and 90% of the extreme absolute value. Contour levels above and below zero are shown as solid and dashed lines, respectively. This allows bright-excitatory (——) and dark-excitatory (---) subregions to be easily distinguished in the contour maps.

For some cells, spatiotemporal receptive-field profiles are obtained with the use of a one-dimensional (1-D) variant of the reverse correlation algorithm. In this case, the stimuli are long, thin bars (typically 15–20° in length × 0.2–0.5° in width), and the stimulus grid is one-dimensional (along X). Effectively, this amounts to eliminating the Y-dimension of the three-dimensional data set (see Fig. 3). This reduction of information is not problematic here because we are mainly interested in the X-T profile and not the X-Y plane (i.e., in constructing the X-T profiles, we integrate along the Y dimension, anyway). The benefit of this 1-D algorithm is that, compared with short bars, long bars often elicit a much stronger response from the neuron being tested, allowing us to obtain X-T profiles for many cells that respond poorly to the full 2-D stimulus ensemble. The 1-D reverse correlation algorithm is used most often with kittens, because the responsivity of cells in kittens is generally much lower than that in adults (e.g., Freeman and Ohzawa 1992). Another advantage of the 1-D variant is that a good X-T profile can be obtained in a fraction of the time required for the 2-D reverse correlation.

Spectral analysis

To evaluate the spatial and temporal frequency selectivities of simple cells, we have performed Fourier analysis on the measured spatiotemporal (X-T) receptive-field profiles. This operation converts a function of space and time into a function of spatial frequency and temporal frequency (see, for example, Bracewell 1978). For each cell, an appropriate time epoch is carefully selected to contain the entire response profile (e.g., Fig. 4*A*). If the time epoch is too short, some of the receptive field will be missing, and the frequency spectrum will not be accurate. If the time epoch is much too long, then the receptive-field profile may not be adequately sampled, and the signal-noise ratio of the X-T data becomes poor. For most cells from adult cats, a 300- to 400-ms time epoch is suitable. For cells from kittens, the time epochs range from 400 to 1,200 ms. Once a time epoch is selected, the X-T data are then zero-padded to fill an array of size 128 × 128. This zero padding is necessary to improve the resolution of the data in the frequency domain. Note that zero padding does not introduce discontinuities (i.e., high-frequency components) into the data because the unpadded X-T profiles have values very close to zero at the borders where zero padding takes place. After padding, a 2-D (128 × 128 point) Fast Fourier Transform (FFT) algorithm is applied to the data. In standard fashion, the amplitude spectrum, $A(sf, tf)$, is computed as

$$A(sf, tf) = \sqrt{\text{Real}(sf, tf)^2 + \text{Imag}(sf, tf)^2} \quad (1)$$

where sf denotes spatial frequency and tf denotes temporal frequency. Real(sf, tf) and Imag(sf, tf) are the real and imaginary

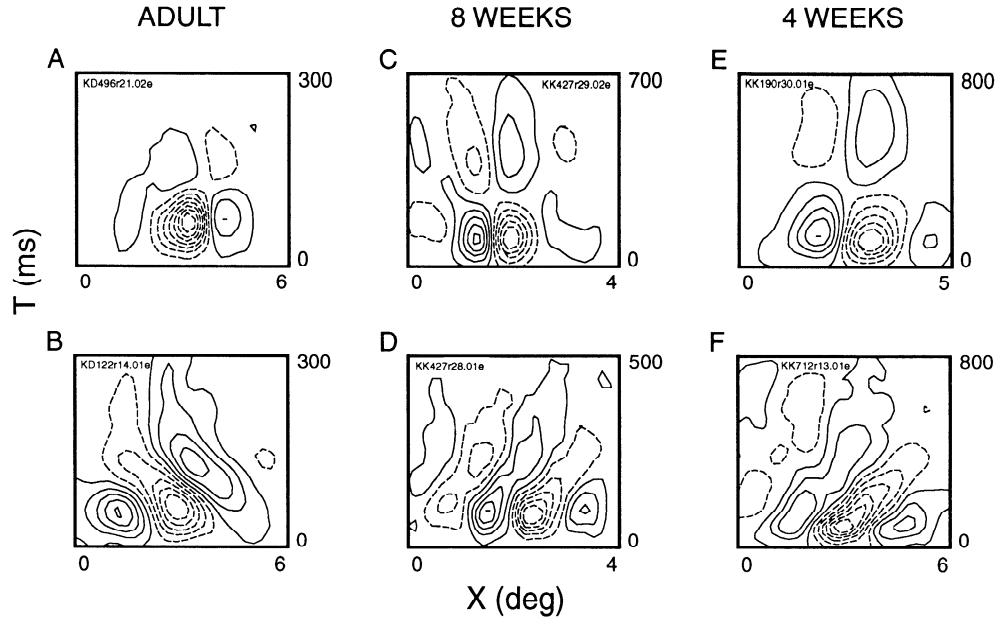

FIG. 4. Representative spatiotemporal receptive-field (X-T) profiles obtained from adult cats (A and B), 8-wk-old kittens (C and D), and 4-wk-old kittens (E and F). The spatial extent (X) of each profile is indicated along the horizontal axis, and the temporal extent (T) is indicated along the vertical axis. Note the large difference in time scale between the adult and kitten examples. Neurons in A, C, and E have X-T profiles that are approximately space-time separable. Neurons in B, D, and F have X-T profiles that are clearly oriented in space-time: the cell shown in B prefers leftward motion, whereas the cells shown in D and F prefer rightward motion (with respect to the axis of the cell's preferred orientation).

parts, respectively, of the Fourier transform. An example amplitude spectrum is shown in Fig. 11B.

RESULTS

For this study, spatiotemporal receptive-field profiles have been obtained for 91 simple cells from 15 adult cats, 63 simple cells from 4 kittens at 8 wk postnatal, and 79 cells from 11 kittens at 4 wk postnatal. Cells were classified as *simple* if they had discrete "ON" and "OFF" receptive-field subregions (Hubel and Wiesel 1962) *and* exhibited a high degree of modulation (1st harmonic/DC response >1) in response to drifting sinusoidal gratings of spatial frequency higher than the optimal (Skottun et al. 1991). Cells that failed to meet either of these two criteria were classified as *complex* and will not be considered further here (see DISCUSSION).

Figure 4 shows spatiotemporal receptive-field profiles (X-T plots) for a representative group of simple cells from adult cats (A and B), 8-wk kittens (C and D), and 4-wk kittens (E and F). Each X-T profile is obtained by stimulation of the dominant eye, while the nondominant eye views a blank screen of equal mean luminance. Spatial position (X) is plotted along the horizontal axis, and time (T) is plotted on the vertical axis. In each profile the areas delimited by solid contour lines have positive values and represent bright-excitatory (or ON)[1] receptive-field subregions. Areas marked by dashed contours have negative values and represent dark-excitatory (or OFF) receptive-field subregions. The relative strengths of bright- and dark-excitatory subregions can be judged by the number of contour lines that delimit these regions (each X-T profile has 10 equally spaced contour levels).

As illustrated by Fig. 4, X-T profiles obtained from adults and kittens demonstrate a variety of shapes. A, C, and E show X-T profiles that are approximately *separable* in the space-time domain. In these cases, the 2-D profile, $R(X, T)$, can be well approximated as the product of two 1-D profiles, one a function of space, $G(X)$, and the other a function of time, $H(T)$ [i.e., $R(X, T) = G(X)H(T)$]. Along the spatial dimension (X), these profiles typically exhibit two or three alternating bright- and dark-excitatory receptive-field subregions (i.e., they are usually bipartite or tripartite). We have, however, measured spatiotemporal response profiles with as many as five or six spatially discrete subregions (see Fig. 8E). Along the temporal dimension (T), separable X-T profiles are typically biphasic (see A, C, and E). However, some cells have X-T profiles that are monophasic in time, and others are triphasic.

In contrast to the data shown in Fig. 4, A, C, and E, the X-T profiles shown in B, D, and F are clearly space-time *inseparable*. Here, we cannot approximate the spatiotemporal response profile as the product of two 1-D functions. In these cases the individual bright-excitatory and dark-excitatory subregions (—— and – – –, respectively) are noticeably oriented, or "tilted," in the space-time domain (see also McLean and Palmer 1989). For these cells, a particular spatial location within the receptive field cannot be assigned, unambiguously, to either an ON subregion or an OFF subregion. Although this appears to violate the original definition of simple cells, as outlined by Hubel and Wiesel

[1] Several studies (e.g., Ferster 1988; Heggelund 1986; Palmer and Davis 1981) have shown that ON regions evoke excitation when probed with a bright stimulus and inhibition when probed with a dark stimulus. Similarly, OFF regions yield excitation in response to a dark stimulus and inhibition in response to a bright stimulus. As a result, ON regions may be referred to as bright-excitatory and OFF regions as dark-excitatory. We shall use the terms ON/OFF and bright-excitatory/dark-excitatory interchangeably throughout this paper.

(1959, 1962), cells B, D, and *F* of Fig. 4 are *not* complex cells. Segregated bright- and dark-excitatory subregions are clearly visible when one views these receptive fields in the joint space-time domain (see DISCUSSION for more on this point).

Because of space-time inseparability, we would expect the cells shown in *B, D,* and *F* to show some preference for the direction of movement of a visual stimulus (Adelson and Bergen 1985; McLean and Palmer 1989; Watson and Ahumada 1983, 1985). All three of these neurons were, in fact, highly direction selective when tested with a drifting sinusoidal grating stimulus. In contrast, the neurons shown in *A, C,* and *E* exhibited little direction selectivity in response to drifting gratings. The relationship between space-time inseparability and direction selectivity is examined quantitatively in the companion paper (DeAngelis et al. 1993).

In general, there is a strong *qualitative* similarity between the *X*-*T* profiles obtained from adult cats and kittens at 4 or 8 wk postnatal. This is evident in Fig. 4 and applies to the vast majority of cells recorded from the three age groups. In each group, we find cells with separable *X*-*T* profiles, as well as those that exhibit varying degrees of inseparability. Moreover, in all groups, we find various types of spatial symmetry, as described below (see Figs. 8 and 9). The most noticeable difference between *X*-*T* profiles from adults and kittens lies in the temporal duration of the responses (note the time scales in Fig. 4). For the neurons shown in Fig. 4, *A* and *B,* the entire spatiotemporal response profile is contained within a time epoch of 300 ms. This is typical of simple cells from adult cats. By contrast, the *X*-*T* profiles shown in *E* and *F* fill a time epoch of 800 ms. Overall, the profiles obtained from 4-wk kittens and 8-wk kittens typically persist for much longer than those from adults, as is shown in the following section.

Temporal receptive-field structure

To quantify differences in temporal structure between adult and kitten *X*-*T* profiles, we have examined both the latency and the duration of these responses. We first consider the measurement of response latency, as illustrated in Fig. 5. Figure 5*A* shows the *X*-*T* profile for a simple cell from an adult cat. For any given value of *T*, we can extract a 1-D spatial receptive-field profile by slicing through the *X*-*T* plot parallel to the *X* axis. Clearly, for $T = 0$ ms or $T \gg 200$ ms, the 1-D receptive-field profile will have no discernible structure. For intermediate values of *T*, however, the 1-D profile exhibits a familiar alternating arrangement of bright- and dark-excitatory subregions, which is typical of simple cells (e.g., Movshon et al. 1978a). This is illustrated in Fig. 5*A, right,* for three values of *T* ($T = 38$ ms, $T = 68$ ms, and $T = 98$ ms). Note that the arrangement and relative strengths of the bright- and dark-excitatory subregions change very little as a function of *T*, that is, the *X*-*T* profile is approximately space-time separable. Note also, however, that the total area under the 1-D receptive-field profile (shown shaded in Fig. 5*A*) changes markedly with *T*. As a measure of the rapidity with which the cell's response follows the onset of a stimulus, we define the peak response latency (T_{peak}) as the value of *T* at which the 1-D receptive-field profile has maximal area under the curve. For the cell of Fig. 5*A*, $T = 68$ ms yields the 1-D receptive-field profile having the largest area under the curve; thus, for this cell, the response latency (T_{peak}) is 68 ms. It should be noted that T_{peak} is not truly a latency, because the cell begins to respond much earlier. Nevertheless, this parameter is convenient for comparing the time course of responses of simple cells from adults and kittens.

Figure 5*B* shows the distribution of T_{peak} for a population of 91 simple cells from adult cats (■), 63 simple cells from 8-wk-old kittens (□), and 79 simple cells from 4-wk-old kittens (□). On average, T_{peak} is 68.2 ms for cells from adults (➡), 90.7 ms for cells from 8-wk kittens (⇨), and 114 ms for cells from 4-wk kittens (⇨). A one-way analysis of variance (ANOVA) reveals a significant main effect ($F_{2,230} = 66.1$, $P < 0.001$) of age on the distribution of T_{peak}. Figure 5*C* shows the mean value of T_{peak} plotted as a function of age, with error bars denoting the 95% confidence interval for each mean. Statistical analysis (Tukey's HSD test) reveals that the differences in T_{peak} between age groups are significant.

It is clear from Fig. 5*C* that the response latency of simple cells declines progressively as a function of age. In addition, the data of Fig. 4 show that the receptive fields of neurons from kittens have a much longer time *duration* than those from adults. To compare the time duration of receptive fields from adults and kittens, we have performed the analysis shown in Fig. 6. To illustrate this analysis, consider the cell depicted in Fig. 6, *A* and *B*. We first find the spatial position (*X*) at which the *X*-*T* profile has its largest positive (or negative) value. This position is indicated by a vertical line through the *X*-*T* profile of Fig. 6*A*. A temporal response curve, $R(T)$, is then obtained by slicing through the *X*-*T* profile parallel to the *T* axis. $R(T)$ is shown as the dashed curve in Fig. 6*B*. Note that $R(T)$ has an initial negative (dark-excitatory) phase, followed by a large positive (bright-excitatory) phase and, finally, a small negative phase.

To quantify the temporal extent of the receptive field, we wish to measure the duration of the temporal response, $R(T)$. However, this is somewhat difficult, because the shape of this curve varies from cell to cell, and there is no obvious functional form that generally describes the curve. One way to deal with this problem is to obtain the *envelope* of the temporal response. This envelope (shown as the solid curve in Fig. 6*B*) is computed as follows (see also Field and Tolhurst 1986). First, the Hilbert transform of the temporal response curve, $H[R(T)]$, is obtained by shifting the phase of all frequency components by 90° (Bracewell 1978; Gabor 1946). The result of this transformation is shown in Fig. 6*B* as the dotted curve. The temporal response curve, $R(T)$, and its Hilbert transform, $H[R(T)]$, are said to form a *quadrature pair.* The envelope of the cell's temporal response, $E(T)$ (solid curve), is computed as the vector sum of these two quadrature components

$$E(T) = \sqrt{R(T)^2 + H[R(T)]^2} \qquad (2)$$

From $E(T)$, it is convenient to define the time duration, *D*, of the receptive field as the width of the envelope at some

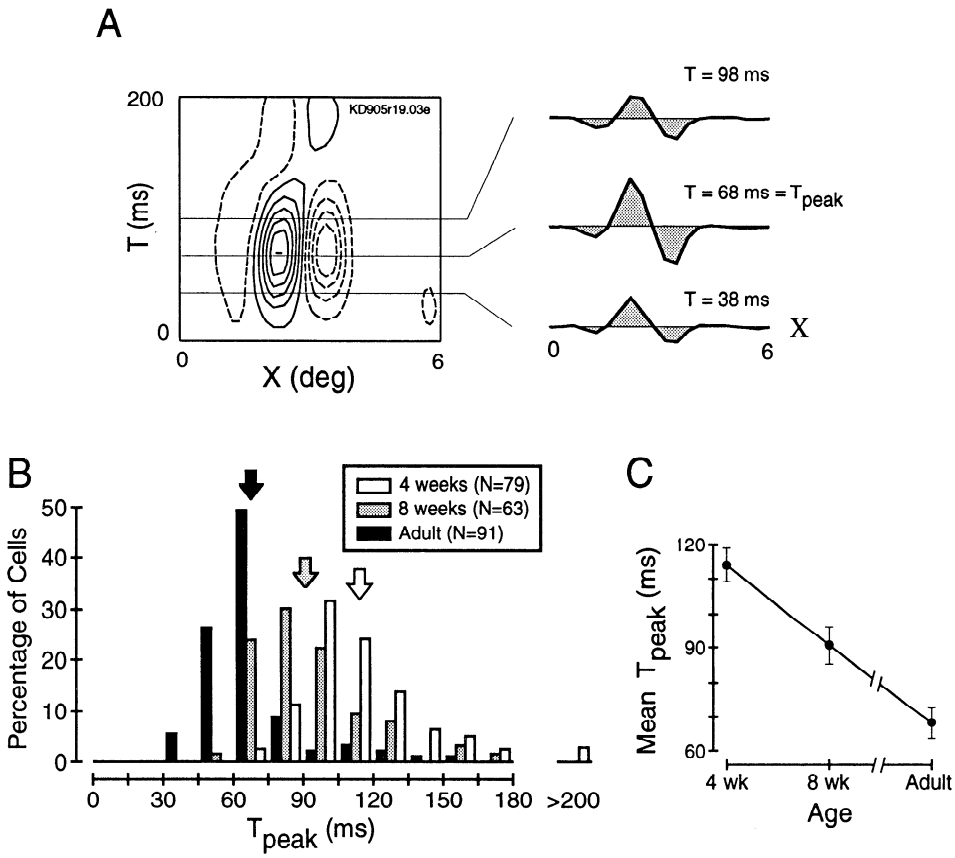

FIG. 5. Analysis of temporal response latency for simple cells from adults and kittens. *A*: an X-T plot is shown for a simple cell from an adult cat. Slicing through the X-T plot at any particular value of T yields a 1-dimensional (1-D) receptive-field profile. Examples are shown on the *right* of *A* for values of T = 38, 68, and 98 ms. Latency to peak response, T_{peak}, is defined as the value of the reverse correlation delay, T, which yields the 1-D receptive-field profile having maximal area under the curve (shaded area). The value of T_{peak} for this cell is 68 ms. *B*: distribution of T_{peak} is shown for populations of simple cells from adult cats (■), 8-wk-old kittens (□), and 4-wk-old kittens (□). Arrows indicate the mean values of T_{peak} for each of the 3 age groups. *C*: mean value of T_{peak} is plotted as a function of age. Error bars denote the 95% confidence interval for each mean value.

criterion response level. To be consistent with spatial envelope measurements described below, we have computed the width of the temporal envelope at the level which is $1/e$ (or 0.367) of the peak envelope value. For the cell of Fig. 6, *A* and *B*, the receptive-field duration, measured in this manner, is D = 145 ms.

Figure 6, *C* and *D*, illustrates the results of this analysis for another simple cell, this one from a 4-wk-old kitten. Note the exceptionally long duration of the temporal envelope shown in Fig. 6*D*. This cell, in fact, had the longest duration receptive field (D = 660 ms) of all those that we have recorded. Note also that the temporal response envelope rises quickly to a peak and then decays slowly. This is a common feature of the temporal receptive-field structure of most cells that we have studied.

The histogram of Fig. 7*A* shows the distribution of receptive-field duration, D, for the same populations of cells as in Fig. 5*B*. The average values of D are 139.6 ms for adults (➡), 211 ms for 8-wk kittens (⇨), and 242.4 ms for 4-wk kittens (⇨). ANOVA shows a significant main effect ($F_{2,230}$ = 49.5, $P < 0.001$) of age on the average value of receptive-field duration. Figure 7*B* shows the mean value of D plotted as a function of age. Tukey's HSD test reveals that each of the mean values is significantly different from the others. Note, however, that the average value of receptive-field duration for 8-wk-old kittens is much closer to that for 4-wk-old kittens than to that for adults.

Spatial receptive-field structure

In the previous section we examined the temporal structure of simple-cell receptive fields from adults and kittens. In this section we compare the spatial organization of receptive fields in these same age groups. To characterize the spatial structure of simple receptive fields, we perform the fitting procedure illustrated in Fig. 8. Shown in Fig. 8*A* is the X-T profile for a simple cell from an 8-wk-old kitten. Slicing through the X-T profile at $T = T_{peak}$ yields a 1-D spatial receptive-field profile, which is shown in Fig. 8*B* by the filled circles. This profile has a central bright-excitatory (ON) subregion, flanked on either side by a dark-excitatory (OFF) subregion.

To compare the structure of 1-D receptive-field profiles from different cells, we have fit these data with a Gabor function (Gabor 1946; Marcelja 1980), which is simply a sinusoid modulated in space by a Gaussian envelope. The Gabor function is chosen because it has a simple mathematical form, and also because it provides a good fit to measured receptive-field profiles (DeAngelis et al. 1991; Field and Tolhurst 1986; Jones and Palmer 1987b). Although other functions might provide a slightly better fit to the data (see Stork and Wilson 1990), the Gabor function is preferable because it has parameters that are easy to interpret and directly relevant to the shape of the receptive-field profile. In this study we have fit 1-D receptive-field profiles with a Gabor function having the form

$$G(x) = Ke^{-[2(x-x_0)/w]^2} \cos(2\pi f_{opt}(x - x_0) + \Phi) \quad (3)$$

where K, x_0, w, f_{opt}, and Φ are free parameters. Specifically, x_0 is the spatial coordinate corresponding to the center of the receptive-field envelope, w is a measure of the width of the receptive-field envelope, f_{opt} is the optimal spatial frequency for the cell, and Φ is the spatial phase of the receptive-field profile with respect to the center of the Gaussian envelope. K is simply a scaling factor. The solid curve in

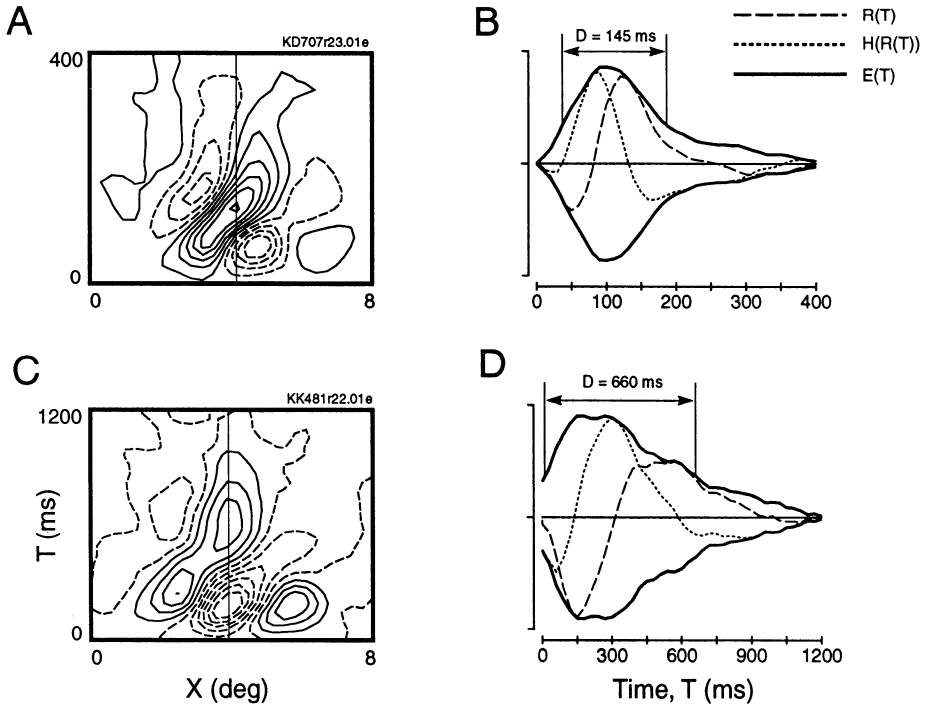

FIG. 6. Examples of the Hilbert transform analysis for computing temporal response envelopes. *A*: an X-T profile is shown for a direction-selective simple cell from an adult cat. *B*: a temporal response curve, $R(T)$ (---), is obtained by slicing through the X-T profile at the X-coordinate indicated by the vertical line in *A*. The temporal response curve, $R(T)$, and its Hilbert Transform, $H[R(T)]$ (· · ·), are said to form a quadrature pair. The temporal response envelope, $E(T)$ (solid curve) is computed as the vector sum of $R(T)$ and $H[R(T)]$, as formulated in *Eq. 2*. The receptive-field duration, D, for this cell is 145 ms. *C*: this X-T profile from a 4-wk-old kitten shows the longest temporal response we have observed. *D*: computation of the temporal envelope, $E(T)$, for the X-T profile shown in *C*. Note the exceptionally long duration (D = 660 ms) for this cell. Notice also that the temporal envelope shown here does not fall to 0 at $T = 0$ ms [i.e., $E(0) \neq 0$]. This should not be interpreted as meaning that the cell produces some instantaneous response to the stimulus, because this is not possible. Rather, this is a consequence of the fact that the Hilbert transform is noncausal. Thus, although $R(0) = 0$ in *D*, $H[R(0)] \neq 0$. However, this artifact has no effect on the measured value of the duration, provided that the value of the envelope at $T = 0$, $E(0)$, is less than or equal to the criterion response level ($1/e$ of the peak value). For virtually all cells in our sample, this latter requirement holds, and the duration, D, can be measured in exactly the same manner as described for the cell in *A* and *B*.

Fig. 8*B* is the Gabor function, $G(x)$, which best fits the 1-D receptive-field profile for this cell. The dashed curve shows the Gaussian envelope of the Gabor function.

Once a Gabor function is fit to the receptive-field profile, the size of the receptive field is given by the spatial extent of the Gaussian envelope. By definition, we use the parameter w (see *Eq. 3*) as a measure of the size of the receptive field. This parameter corresponds to the width of the Gaussian envelope at a criterion response level that is $1/e$ (or 0.367) of the peak height of the envelope. For the cell of Fig. 8*B*, the width of the receptive field is $w = 2.7°$. Figure 8*C* shows the distribution of receptive-field envelope width, w, for simple cells from adult cats and kittens. The mean values of w are 1.95° for adults (➡), 2.03° for 8-wk kittens (⇨), and 2.62° for 4-wk-old kittens (⇨). A one-way ANOVA reveals a significant main effect of age ($F_{2,230} = 11.98$, $P < 0.001$). Mean values and 95% confidence intervals are plotted in Fig. 8*D* as a function of age. Tukey's HSD test shows that the mean envelope width for 4-wk kittens is significantly larger than that for 8-wk kittens or adult cats. How-

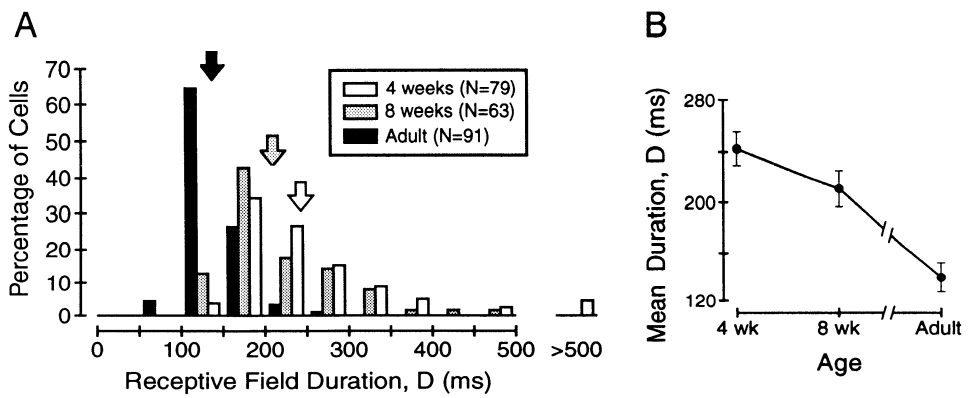

FIG. 7. Summary of receptive-field duration, D, for simple cells from animals of different ages. *A*: histogram is shown of the distributions of D for adults (■), 8-wk-old kittens (□), and 4-wk-old kittens (□). Mean values for these populations are indicated by the arrows. *B*: mean receptive-field duration, D, is plotted as a function of age. Error bars represent the 95% confidence interval for each mean value.

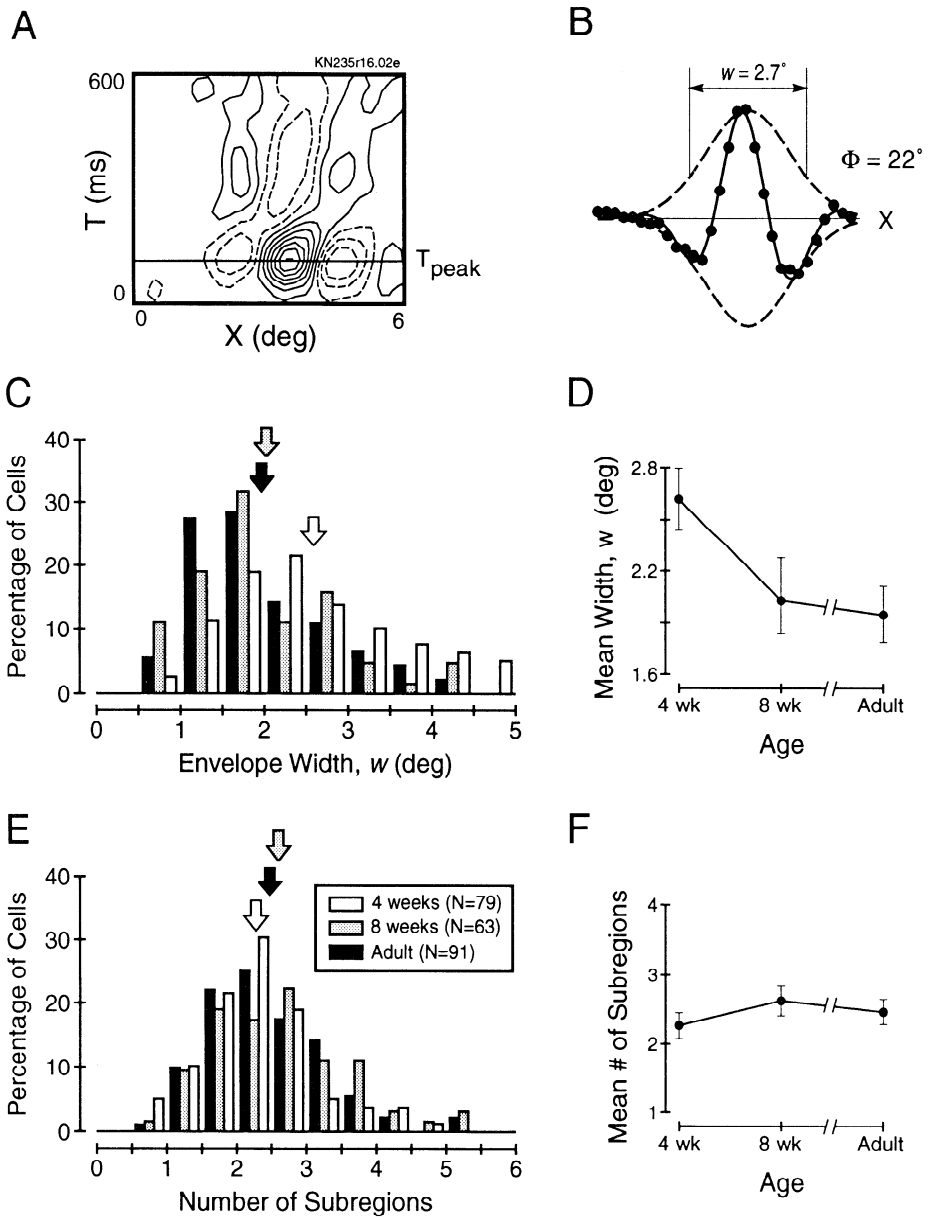

FIG. 8. Analysis of receptive-field size and periodicity is illustrated here. *A*: *X*-*T* plot is shown for a simple cell from an 8-wk-old kitten. Horizontal line through the *X*-*T* profile indicates the optimal reverse correlation delay (T_{peak}) for this cell. *B*: a 1-dimensional (1-D) spatial receptive-field profile is obtained by slicing through the *X*-*T* plot at $T - T_{peak}$. This 1-D profile is shown as filled circles. The solid curve is the Gabor function (see *Eq. 3*) that best fits the 1-D spatial receptive-field profile. Dashed curves show the Gaussian envelope of this function. The best-fitting Gabor function has an envelope width, w, of 2.7°. The spatial phase, Φ, of the Gabor function, relative to the center of the Gaussian envelope, is $\Phi = 22°$. *C*: histogram showing the distribution of receptive-field envelope width, w, for populations of simple cells from adult cats (■), 8-wk-old kittens (□), and 4-wk-old kittens (□). *D*: mean value of w is plotted as a function of age, with error bars indicating the 95% confidence interval for each value. *E*: distribution of the number of subregions within the receptive fields of simple cells from each of the 3 age groups. Number of subregions is computed by *Eq. 4* (see text for details). *F*: mean number of subregions is plotted as a function of age, showing that the periodicity of simple receptive fields changes little with age after 4 wk postnatal.

ever, the mean value of w for 8-wk kittens is indistinguishable from the mean for adult cats. Comparison of Fig. 8*D* with Fig. 7*B* elucidates a fundamental difference in the development of spatial and temporal receptive-field structure. Although the spatial envelope of the receptive field decreases to adult size by 8 wk postnatal, the temporal envelope is still much longer for 8-wk kittens than for adult cats. Thus it is clear that the spatial dimension of the receptive field matures more rapidly than the temporal dimension.

Another interesting parameter to examine is the number of subregions within the 1-D receptive-field profile. This is computed as follows

$$\text{Number of subregions} = \sqrt{3} \times w \times f_{opt} \times 2 \qquad (4)$$

where w and f_{opt} are parameters of the Gabor function, as formulated in *Eq. 3*. $\sqrt{3}w$ corresponds to the width of the Gaussian envelope at a criterion level that is 5% of the peak amplitude. Multiplying $\sqrt{3}w$ by the optimal spatial frequency, f_{opt}, gives the number of cycles within the receptive field. An additional factor of two converts number of cycles into number of subregions. Figure 8*E* shows the distribution of the number of subregions in the receptive fields of simple cells from adult cats and kittens. The distributions from the three age groups overlap almost completely. The mean number of subregions (Fig. 8*F*) is 2.25 for 4-wk kittens, 2.60 for 8-wk kittens, and 2.45 for adult cats; these values are not significantly different (Tukey HSD test). Thus, although the average envelope width decreases with age beyond 4 wk postnatal (Fig. 8*D*), the periodicity of simple cell receptive fields appears mature at 4 wk of age. These two observations suggest that the preferred spatial frequency of simple cells increases from 4 to 8 wk postnatal, as shown below (see Fig. 13*B*).

We now consider the spatial arrangement of bright- and dark-excitatory subregions within the receptive field. In general, we can characterize the spatial organization, or symmetry, of simple cell receptive fields by examining the

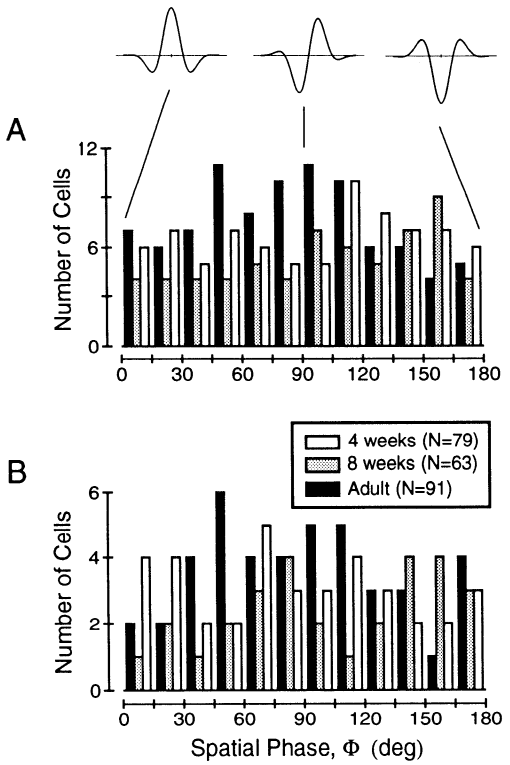

FIG. 9. Summary of receptive-field phase data for simple cells from cats and kittens. *A*: histogram showing the distribution of spatial phase, Φ, for *all* simple cells recorded from adult cats (■), 8-wk-old kittens (□), and 4-wk-old kittens (□). Each value of Φ was obtained through the fitting procedure illustrated in Fig. 8, *A* and *B*. Shown above the histogram are Gabor functions having Φ = 0°, Φ = 90°, and Φ = 180°, respectively (*left* to *right*). *B*: histogram showing the distribution of Φ for the subset of cells with approximately space-time separable receptive fields, as determined by computing a direction selectivity index (DSI, see *Eq. 7*). Only those cells having a DSI < 0.2 are shown in this histogram (n = 43 for adults, n = 29 for 8-wk-old kittens, n = 37 for 4-wk-old kittens). Note that the distribution is approximately uniform (see text for details).

phase parameter, Φ (see *Eq. 3*), of the best-fitting Gabor function (DeAngelis et al. 1991; Field and Tolhurst 1986; Jones and Palmer 1987a). This is illustrated at the top of Fig. 9, which shows Gabor functions having phases of 0, 90, and 180°, respectively (*left* to *right*). When the spatial phase is 0 or 180°, the Gabor function is even-symmetrical; when the phase is 90° (or 270°), the Gabor function is odd-symmetrical. For the receptive field shown in Fig. 8*B*, Φ equals 22°, and the 1-D receptive-field profile is close to even-symmetrical.

The histogram of Fig. 9*A* shows the distribution of receptive-field phase,[2] Φ, for all simple cells recorded from adult cats (n = 91, ■), 8-wk kittens (n = 63, □), and 4-wk kittens (n = 79, □). Clearly, the distribution of Φ is very broad. In fact, for each age group, the distribution of Φ is statistically indistinguishable from uniform (χ^2 = 8.28, P = 0.69 for adults; χ^2 = 5.71, P = 0.89 for 8-wk kittens; χ^2 = 3.47, P = 0.98 for 4-wk kittens). These data agree well with those obtained by Field and Tolhurst (1986), Hamilton et al. (1989), and Jones and Palmer (1987b), despite differences in the methodology used to obtain phase estimates. Note, in particular, that the phase data of Fig. 9*A* are *not* grouped around values of 0 (or 180°) and 90°. Thus the receptive fields of simple cells are not limited to even- and odd-symmetrical types, as some researchers have categorized them (e.g., Kulikowski and Bishop 1981; Movshon et al. 1978a; see Field and Tolhurst 1986 for review). Instead, simple-cell receptive fields exhibit all spatial phases with nearly equal probability. Moreover, simple-cell receptive fields in 4-wk kittens exhibit the full range of symmetries exhibited by cells in adult cats.

[2] Note that the phase axis in Fig. 9 has a range from 0 to 180°. Of course, phase actually varies from 0 to 360°, but we limit the scale because of the confounding effect of orientation. For example, a receptive-field profile having Φ = 90° would become a profile having Φ = 270° if the preferred orientation of the cell was rotated by 180°. Thus we cannot actually distinguish phases ranging from 180 to 360° from those in the 0–180° range. For this reason, values of Φ falling between 180 and 360° have been reflected (around 180°) to fall in the range from 0 to 180°. See Field and Tolhurst (1986) for more on this point.

Spatial symmetry and space-time separability

At this point it is necessary to address a potential problem with the data of Fig. 9*A*. Recall from Fig. 8*A* that the 1-D receptive-field profile for each cell is obtained by slicing through the X-T profile at $T = T_{peak}$. The spatial phase, Φ, is then obtained by fitting a Gabor function to the 1-D receptive-field profile. What happens to the value of Φ if we obtain a 1-D receptive-field profile by slicing through the X-T plot at a different value of T? As shown in Fig. 10, Φ can vary considerably over time if the cell's receptive field is not space-time separable.

Figure 10*A* shows a space-time inseparable receptive-field profile for a direction-selective simple cell. To examine how spatial receptive-field structure changes over time, we slice through the X-T profile at several different values of T, extract 1-D receptive-field profiles, and find the best-fitting Gabor function for each time slice (as in Fig. 8*B*). Figure 10, *C–G*, shows how each of the five parameters of the best-fitting Gabor function (see *Eq. 3*) varies over time. For the cell of *A*, notice that the envelope center (x_0), the optimal spatial frequency (f_{opt}), and the envelope width (w) do not change substantially over time (open circles of Fig. 10, *D–F*, respectively). There is, however, a large gradual change in the phase (Φ) of the receptive field over time (see open circles in *G*). This example demonstrates that cells with space-time inseparable receptive fields do not have a uniquely defined spatial phase (see also Hamilton et al. 1989).

For the simple cell shown in Fig. 10*B*, the receptive-field profile is approximately space-time separable. As for the cell of *A*, the envelope center (x_0), optimal spatial frequency (f_{opt}), and envelope width (w) are approximately independent of T (see filled circles in *D–F*, respectively), although the envelope width does increase somewhat around T = 140 ms, when the envelope amplitude, K, is very small. The main difference between cell *A* and cell *B* can be seen in Fig. 10*G*. Instead of changing gradually with T, the receptive-field phase for cell *B* exhibits a sharp transition between T = 125 ms and T = 140 ms (see filled circles in *G*). Before T = 125 ms, Φ is fairly constant at ~100°. After T = 140 ms, Φ remains fairly constant between 260

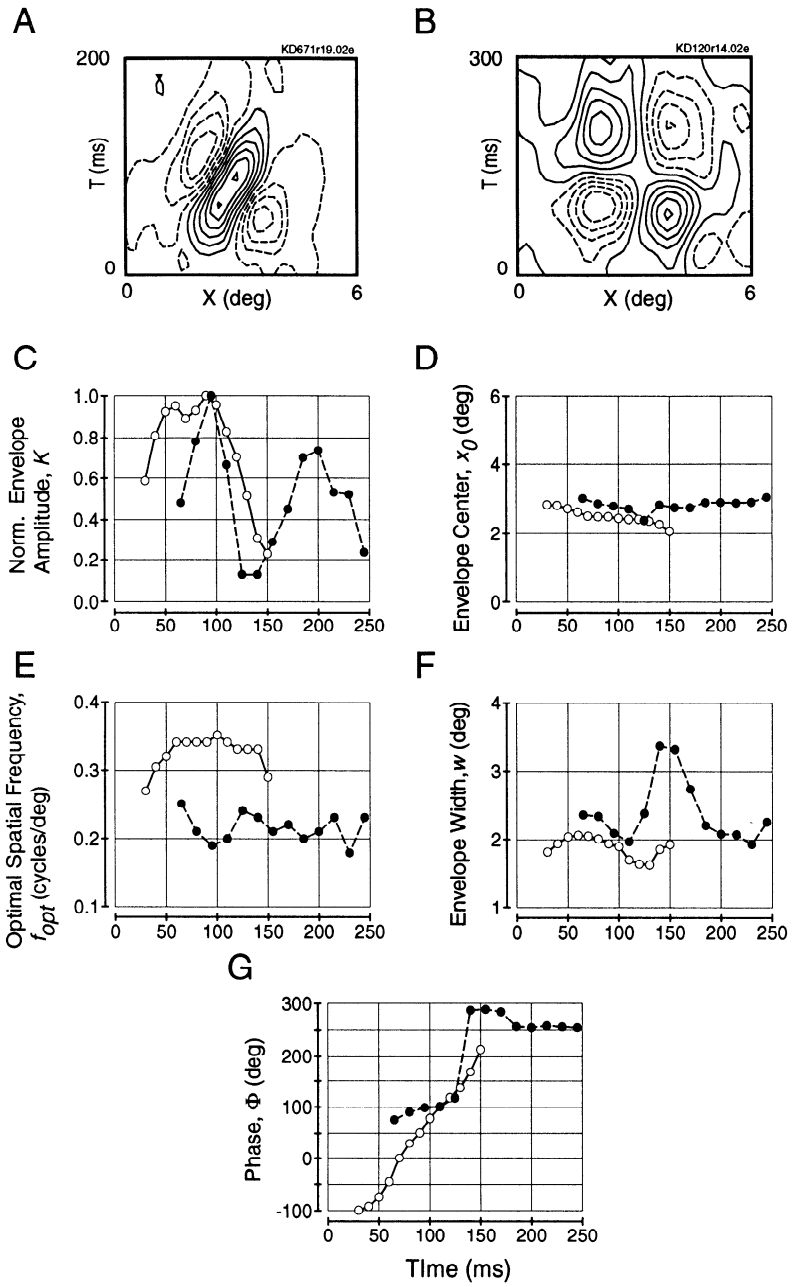

FIG. 10. Analysis of spatial receptive-field structure as a function of time for 2 simple cells. *A*: a space-time inseparable *X-T* profile is shown for a simple cell from an adult cat. Note that the subregions are clearly oriented, or tilted, in space-time. *B*: data are shown for a simple cell that has a space-time separable *X-T* plot. For each of the 2 cells, 1-dimensional (1-D) receptive-field profiles are analyzed over a range of values of *T*. At each value of *T*, a Gabor function is fit to the 1-D receptive-field profile, as shown in Fig. 8, *A* and *B*. *C–G*: 5 parameters (see *Eq. 3*) of the best-fitting Gabor function as a function of time for each of these 2 cells. Data points for the cell shown in *A* are denoted by open circles and connected by solid lines; data for the cell in *B* are shown as filled circles and connected by dashed lines. The 5 parameters plotted are as follows: normalized envelope amplitude, *K* (*C*); envelope center, x_0 (*D*); optimal spatial frequency, f_{opt} (*E*); envelope width, *w* (*F*), and spatial phase, Φ (*G*). Note the patterns of change in Φ as a function of time for each of the 2 cells.

and 280°. The 180° phase jump at $T = 140$ ms can be seen in the *X-T* profile (*B*) as a reversal of polarity from bright-excitatory to dark-excitatory, and vice versa. Thus cells with separable *X-T* profiles have a *unique* spatial phase (± increments of 180°), whereas cells with inseparable *X-T* profiles do not.

The fact that many cells do not have a unique spatial phase raises the possibility that the distribution of Φ (see Fig. 9*A*) only *appears* to be uniform because it includes cells with space-time inseparable receptive fields. Thus the data of Fig. 9*A*, as well as the data from other studies (Field and Tolhurst 1986; Hamilton et al. 1989; Jones and Palmer 1987b), may be misleading. To address this potential problem, we have examined the distribution of spatial phase, Φ, for the subset of neurons that have *X-T* profiles that are space-time separable (or nearly so). Specifically, Fig. 9*B* shows the distribution of Φ for those cells from adults and kittens that have a direction selectivity index (DSI) <0.2 (see *Eq. 7* for the definition of DSI). Cells that meet this criterion have *X-T* profiles that are nearly separable, so that there is an approximately unique spatial phase. The distribution of Φ for these cells, shown in Fig. 9*B*, is again very broad. In fact, for all three age groups, the distribution is indistinguishable from uniform (adults: $\chi^2 = 6.36$, $P = 0.85$; 8-wk kittens: $\chi^2 = 6.21$, $P = 0.86$; 4-wk kittens: $\chi^2 = 3.52$, $P = 0.98$). Thus there are two points that should be emphasized. First, the distribution of spatial phases exhibited by simple cells is approximately *uniform*, regardless of whether one includes direction-selective (i.e., space-time inseparable) receptive fields in the analysis. Hence simple cells do not fall into canonical even- and odd-symmetrical classes. Second, there appears to be no difference in the spatial organization, or symmetry, of receptive fields between kittens and adult cats.

Frequency domain analysis

Thus far we have seen how the course of postnatal development alters some aspects of the temporal and spatial structure of simple-cell receptive fields. Another way to gauge the effects of development on the response properties of these neurons is to examine their stimulus selectivities in the frequency domain (Derrington and Fuchs 1981). In particular, it is of interest to evaluate the ranges of temporal and spatial frequencies that can be encoded by cells in animals of different ages. If we assume that simple cells act as linear spatiotemporal filters, we can obtain estimates of a cell's spatial and temporal frequency selectivities through Fourier analysis of the spatiotemporal receptive-field (X-T) profile. In this section we examine the spatial and temporal frequency tuning of populations of simple cells from 4-wk kittens, 8-wk kittens, and adult cats. The assumption of linearity is addressed in the companion paper (DeAngelis et al. 1993), where it is shown that linear predictions of spatial and temporal frequency tuning are suitably accurate for our purposes here.

Figure 11 illustrates the frequency domain analysis. *A* shows the X-T plot for a direction-selective simple cell from an adult cat. Notice that the receptive field has four clearly defined subregions, all of which are tilted somewhat to the right in space-time. *B* shows a contour map of the spatiotemporal amplitude spectrum, which is obtained through Fourier analysis of the X-T plot (see METHODS). This contour map plots response amplitude as a function of spatial frequency (SF) and temporal frequency (TF). The complete amplitude spectrum consists of four quadrants and is symmetrical about the origin; thus only two of the four quadrants are distinct. Figure 11*B* shows the two quadrants corresponding to positive spatial frequencies. The positive and negative temporal frequency quadrants give the amplitude of the cell's response for motion in the preferred and nonpreferred directions, respectively (see Adelson and Bergen 1985; Watson and Ahumada 1985). For this cell the peak amplitude for positive temporal frequencies is much larger ($\sim$3 times) than the peak amplitude for negative temporal frequencies. This asymmetry in the strength of the response for positive and negative temporal frequencies can be used as an estimate of the cell's directional selectivity (see *Eq. 7* and Fig. 17). Cells with space-time separable X-T profiles have spectra that are identical in amplitude for positive and negative temporal frequencies.

To extract estimates of the cell's spatial and temporal frequency tuning curves, the 2-D spatiotemporal amplitude spectrum is fit with the function

$$A(sf, tf) = A_0 e^{-[(sf-sf_0)/a]^2} \times \frac{c(tf - tf_0)^n e^{-[c(tf-tf_0)]}}{n^n e^{-(n)}} \qquad (5)$$

where sf_0, a, c, tf_0, and n are free parameters. A_0 is determined by the peak amplitude of the 2-D spectrum. This function is simply the product of a Gaussian (in spatial frequency, sf) and a gamma distribution (in temporal frequency, tf). A Gaussian is chosen to fit the spatial frequency dimension because it is known that the envelope of a simple cell's spatial sensitivity profile is approximately Gaussian (Field and Tolhurst 1986; Jones and Palmer 1987a). For the temporal frequency dimension, we have no apriori reason to choose the gamma distribution, other than the fact that it seems to resemble the data. This function is, in fact, quite versatile because it can take on a continuum of shapes ranging from an exponential to a Gaussian, depending on the value of n.

The formulation of *Eq. 5* is fit independently to the positive and negative temporal frequency quadrants of the amplitude spectrum, as shown in Fig. 11*C*. The purpose of fitting this function is to extract spatial and temporal frequency tuning parameters that are less sensitive to noise in the X-T profile. All data points contribute equally to the fit, whereas parameters extracted from the raw profile can be influenced heavily by local features near the points of interest. Figure 11*D* shows the temporal frequency tuning curve that is obtained by slicing through the positive temporal frequency quadrant of the spatiotemporal amplitude spectrum. The solid curve in *D* is a slice, parallel to the temporal frequency axis, through the peak of the best-fitting function (shown in *C*); the dashed curve in *D* is a slice through the peak of the raw amplitude spectrum (shown in *B*). Clearly, the solid curve in *D* provides an acceptable fit to the actual amplitude data. From this fit, we extract the following parameters: the optimal temporal frequency (TF_{opt}), which is the frequency at which the solid curve in *D* has its peak, and the high temporal frequency cutoff (TF_{high}), which is the temporal frequency at which the curve drops to one-half of its peak value. By slicing through the spatiotemporal amplitude spectrum parallel to the spatial frequency axis, we can also obtain an estimate of the cell's spatial frequency tuning curve, as shown in Fig. 11*E*. Again, the solid curve is a section through the 2-D fit. In this case, we extract the optimal spatial frequency (SF_{opt}) and the high spatial frequency cutoff (SF_{high}).

Temporal frequency selectivity

Let us first consider the postnatal development of temporal frequency selectivity, as summarized in Fig. 12. Figure 12*A* shows the distribution of the optimal temporal frequency, TF_{opt}, for adults and kittens. It is clear from this histogram that simple cells from kittens tend to prefer lower temporal frequencies than those from adults. Mean values of TF_{opt} are 2.6 Hz for adults (➡), 1.75 Hz for kittens at 8 wk postnatal (⇨), and 1.42 Hz for kittens at 4 wk postnatal (⇨). Figure 12*B* shows that there is a statistically significant trend (ANOVA: $F_{2,230} = 44.9$, $P < 0.001$) for TF_{opt} to increase as a function of age. Tukey's HSD test reveals that the mean values of TF_{opt} for each age group are significantly different from one another. Note, however, that the mean value of TF_{opt} for 8-wk kittens is much closer to the mean for 4-wk kittens than to that for adults. It should also be noted that the distribution of TF_{opt} for adults is similar to that reported by Baker (1990). To our knowledge, no other temporal frequency tuning data are available for the striate cortex of kittens, although there are some temporal frequency data available for the posteromedial lateral suprasylvian area (PMLS) in kittens (Zumbroich et al. 1988).

The histogram of Fig. 12*C* shows the distribution of the high temporal frequency cutoff, TF_{high}, for the same populations of simple cells as in *A*. This parameter (TF_{high}) can be used as a metric for comparing the highest temporal fre-

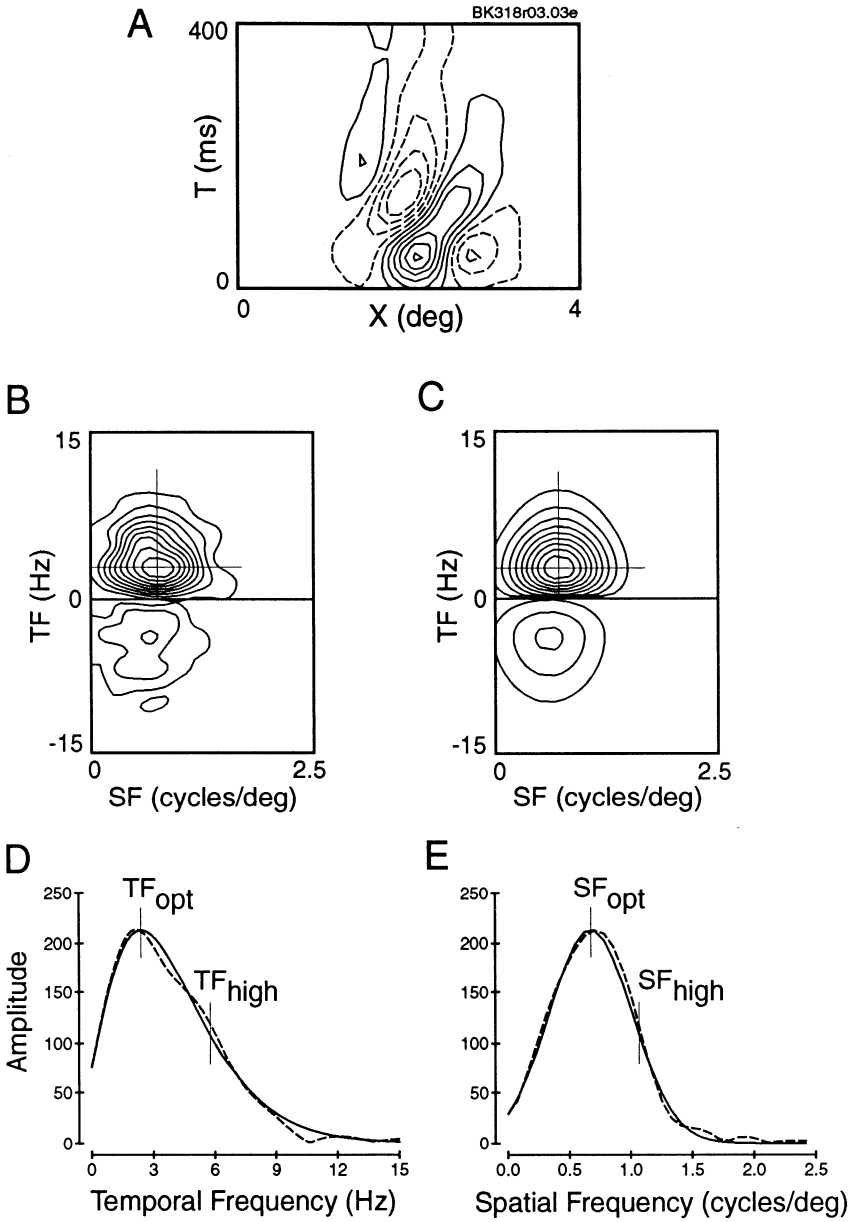

FIG. 11. Frequency domain analysis is illustrated for a simple cell from an adult cat. *A*: *X*-*T* profile. *B*: the spatiotemporal amplitude spectrum is shown for the cell whose *X*-*T* plot is displayed in *A*. The amplitude spectrum is obtained by performing a 2-dimensional (2-D) Fourier Transform, and is plotted as a contour map. Only the positive spatial frequency (SF) quadrants are shown. The amplitude spectrum for positive temporal frequencies (upper quadrant) corresponds to rightward motion in *A*. The negative temporal frequency (TF) quadrant corresponds to leftward motion in *A*. *C*: contour map showing the best fit of *Eq. 5* to the 2-D amplitude spectrum shown in *B*. *D*: temporal frequency tuning curve, as extracted from the 2-D amplitude spectrum. Dashed curve is a slice (parallel to the TF axis) through the peak of the raw spectrum shown in *B*. Solid curve is a similar slice through the peak of the best-fitting surface shown in *C*. Optimal temporal frequency (TF_{opt}) is determined as the temporal frequency at which the solid curve has its peak value. High temporal frequency cutoff (TF_{high}) is defined as the value of TF at which the solid curve drops to ½ of its peak value. *E*: a predicted spatial frequency tuning curve is shown for the same cell. As in *D*, the dashed curve is a slice through the raw amplitude spectrum, and the solid curve is a cross section through the best-fitting surface. SF_{opt} and SF_{high} are defined analogously to TF_{opt} and TF_{high}.

quencies that can be reliably encoded by the cells. The mean values of TF_{high} are 7.2 Hz for cells from adults (➡), 4.7 Hz for cells from 8-wk kittens (⇛), and 4.1 Hz for cells from 4-wk kittens (⇨). The trend for TF_{high} to increase with age (see Fig. 12*D*) is also highly significant (ANOVA: $F_{2,230} = 121.9$, $P < 0.001$). Note again that the mean value of TF_{high} for 8-wk kittens is much closer to the mean for 4-wk kittens than to the mean value for adults. These data show that the immature temporal receptive-field structure of neurons in kittens, namely their prolonged response duration, drastically limits the range of temporal frequencies that can be encoded by these neurons.

Spatial frequency selectivity

The postnatal development of spatial frequency selectivity is summarized in Fig. 13, which has the same format as Fig. 12. The histogram of Fig. 13*A* shows the distribution of optimal spatial frequencies (SF_{opt}). The average values of SF_{opt} are 0.42 cycles/deg for adults (➡), 0.45 cycles/deg for 8-wk kittens (⇛), and 0.26 cycles/deg for cells from 4-wk kittens (⇨). A one-way ANOVA reveals a significant main effect for age ($F_{2,230} = 24.9$, $P < 0.001$); however, Tukey's HSD test shows that only the 4-wk kittens have a mean that is significantly different from the other groups. The mean values of SF_{opt} for 8-wk kittens and adults are not significantly different (see Fig. 13*B*). It should be noted that the average values of SF_{opt} for our 4- and 8-wk-old kittens agree quite well with the data reported by Derrington and Fuchs (1981). Moreover, the distribution of optimal spatial frequencies for our adult cats is similar to those reported by Baker (1990), Ferster and Jagadeesh (1991), and Holub and Morton-Gibson (1981). However, our mean optimal spatial frequency for adults is considerably lower than that reported for simple cells by Movshon et al. (1978c). This discrepancy probably arises because we sam-

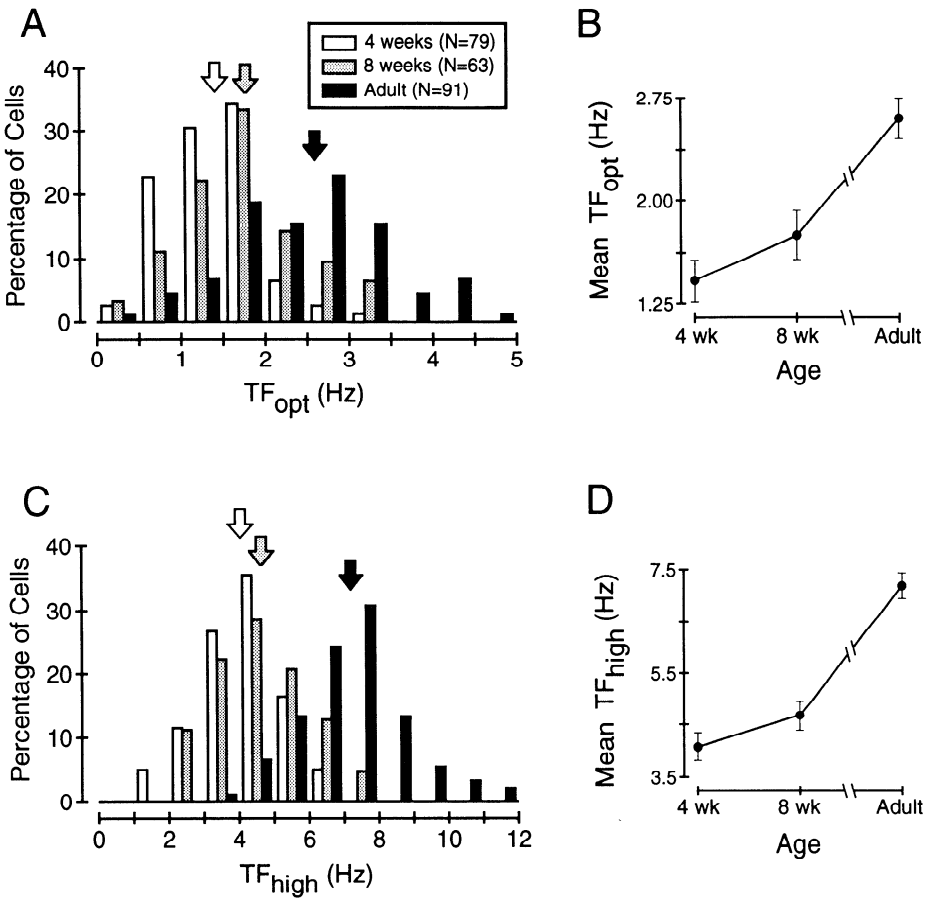

FIG. 12. Summary of the postnatal development of temporal frequency selectivity. *A*: histogram is shown of the distribution of optimal temporal frequencies (TF_{opt}) for populations of cells from adult cats (■), 8-wk-old kittens (□), and 4-wk-old kittens (□). Mean values are indicated by arrows. *B*: mean TF_{opt} is plotted as a function of age, with error bars denoting the 95% confidence interval for each mean value. *C*: histogram showing the distribution of high temporal frequency cutoffs (TF_{high}) for the same populations of cells shown in *A*. *D*: mean TF_{high} is plotted as a function of age.

ple cells over a larger range of eccentricities than did Movshon et al. (1978c) (see DISCUSSION).

Figure 13*C* shows the distribution of the high spatial frequency cutoffs, SF_{high}, for the same populations of cells from adults and kittens. The mean values of SF_{high} are 0.71 cycles/deg for cells from adults (➡), 0.72 cycles/deg for cells from 8-wk kittens (⇨), and 0.47 cycles/deg for cells from 4-wk kittens (⇨). There is a significant trend (ANOVA: $F_{2,230} = 22.6$, $P < 0.001$) for SF_{high} to increase with age (see Fig. 13*D*); however, the distributions of SF_{high} for adults and 8-wk kittens are not significantly different.

Overall, the histograms of Figs. 12 and 13 show that simple cells from 4-wk-old kittens respond to a more limited range of both temporal and spatial frequencies than simple cells of adult cats. However, there is a clear difference in the *time course* of development for temporal frequency tuning and spatial frequency tuning. For 8-wk-old kittens, spatial frequency selectivity (Fig. 13, *B* and *D*) has clearly reached adult levels of specificity, whereas temporal frequency tuning (Fig. 12, *B* and *D*) remains highly immature. These observations demonstrate clearly that spatial selectivity matures earlier than temporal selectivity.

Joint spatial and temporal frequency distribution

In the previous sections, we have seen how the distributions of optimal spatial and temporal frequencies change during postnatal development. Thus far we have only considered these parameters independently. In this section we examine the joint distribution of optimal spatial and temporal frequencies. Viewing the data in this manner gives further insight into the developmental dynamics that take place in the kitten's visual cortex.

Figure 14*A* shows the joint distribution of TF_{opt} and SF_{opt} for the population of 91 simple cells recorded from adult cats. In this scatter plot, each point represents one neuron. Note that there is a clear negative correlation ($r = -0.57$) between TF_{opt} and SF_{opt}, such that neurons tuned to low spatial frequencies tend to prefer high temporal frequencies, and vice versa. This trend is statistically significant ($t = 6.55$, $P < 0.001$). A similar finding has been reported by Baker (1990), although he found a somewhat weaker correlation between TF_{opt} and SF_{opt}. Figure 14, *B* and *C*, shows the joint frequency distributions for 8- and 4-wk-old kittens, respectively. Unlike the data from adult cats, there is no clear relationship between TF_{opt} and SF_{opt} for kittens. For the 8-wk-old kittens (*B*), there is a weak negative correlation ($r = -0.11$), but this is not significant ($t = 0.85$, $P = 0.40$). There is no correlation between TF_{opt} and SF_{opt} for the 4-wk-old kittens ($r = 0.013$).

From the data of Figs. 12 and 13, it is clear that spatial frequency selectivity matures before temporal frequency selectivity. Figure 14 shows that this development is approximately a two-stage process. From 4 (*C*) to 8 wk postnatal (*B*), the predominant change in the joint frequency distribution is a spreading of points along the spatial frequency axis. During this period the range of optimal spatial frequencies increases considerably, whereas the range of optimal temporal frequencies changes only slightly. From 8 wk

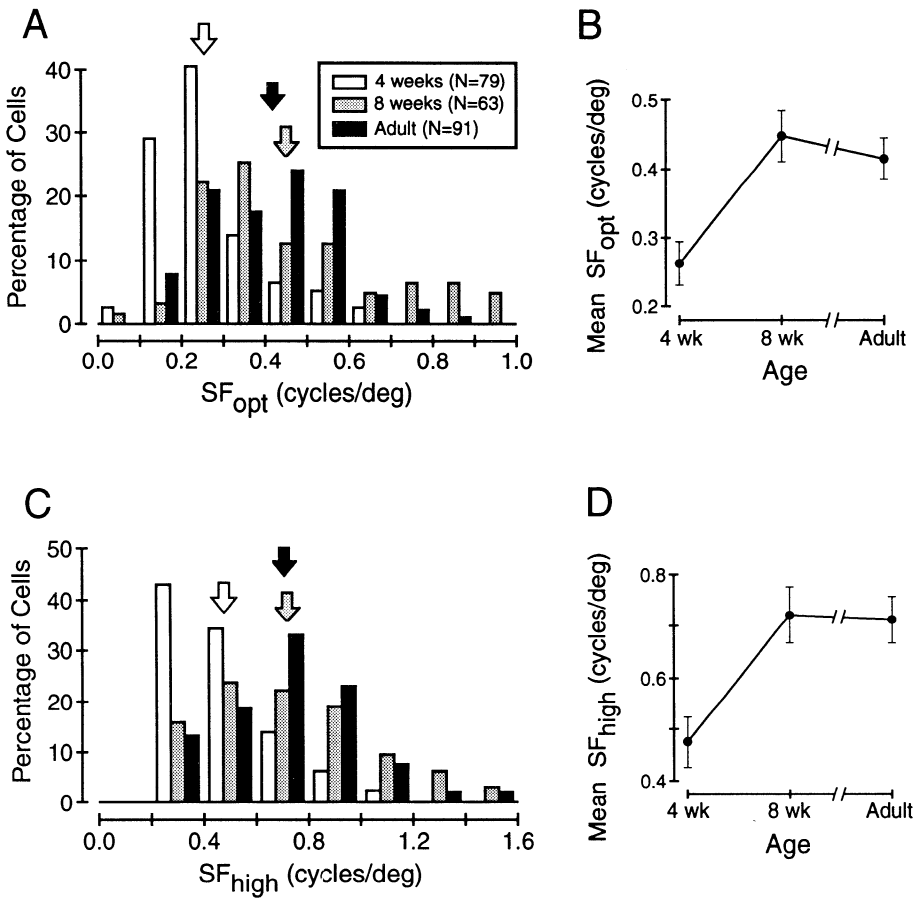

FIG. 13. Summary of developmental changes in spatial frequency selectivity. Format of this figure is identical to that of Fig. 12. Distributions of optimal spatial frequencies (SF_{opt}) and high spatial frequency cutoffs (SF_{high}) are shown in *A* and *C*, respectively. Mean values of SF_{opt} and SF_{high} are plotted as a function of age in *B* and *D*.

postnatal (*B*) until adulthood (*A*), a second stage of development occurs that is spatial frequency specific. During this time, cells tuned to low spatial frequencies (i.e., <0.4 cycles/deg) show a large shift toward higher temporal frequencies, whereas cells tuned to high spatial frequencies (i.e., >0.4 cycles/deg) show little change in their optimal temporal frequencies.

To analyze this spatial frequency–specific shift in TF_{opt} more quantitatively, each of the three populations of simple cells has been split into two groups: *1*) cells tuned to spatial frequencies <0.4 cycles/deg (the "low SF_{opt}" group), and *2*) cells tuned to spatial frequencies >0.4 cycles/deg (the "high SF_{opt}" group). For each spatial frequency group, we analyze the distribution of TF_{opt} as a function of age, as done in Fig. 12. For the high SF_{opt} group, there is no significant trend (ANOVA: $F_{2,85} = 3.0$, $P = 0.06$) for TF_{opt} to change as a function of age. In contrast, a one-way ANOVA for the low SF_{opt} group reveals a highly significant trend ($F_{2,142} = 83.7$, $P < 0.001$) for TF_{opt} to increase with age. This is due mainly to the large mean value of TF_{opt} for adults (see Fig. 14*A*). At 4 wk postnatal, the mean values of TF_{opt} for the low and high SF_{opt} groups (1.41 and 1.48 Hz, respectively) are not significantly different (Tukey's HSD test). The same is true at 8 wk postnatal (mean values of TF_{opt} are 1.80 and 1.69 Hz, respectively, for the low and high SF_{opt} groups). For adults, however, the low SF_{opt} group has a significantly higher mean TF_{opt} (3.25 Hz) than does the high SF_{opt} group (2.02 Hz). These results show that developmental changes in temporal frequency tuning are specific for spatial frequency. Hence the mechanisms that account for the overall change in TF_{opt} with age (Fig. 12) mainly affect those cells that are tuned to low spatial frequencies.

Population response

In the previous sections, we have characterized the spatial and temporal frequency selectivity of individual simple cells from cats and kittens. We now extend this analysis to obtain a spatiotemporal frequency response for populations of simple cells from adults and kittens. Such a population response should reflect the full range of spatial and temporal frequencies that can be encoded by simple cells in the striate cortex. The population response may then be compared with behavioral contrast sensitivity data, given some simple assumptions.

The rationale for constructing a population response is simple. Individual neurons are generally tuned to a small range of spatial and temporal frequencies. Some cells respond best when stimulated with a low spatial frequency and a high temporal frequency, whereas others respond best to high spatial and low temporal frequencies. By considering the responses of a representative population of cells, we can estimate the entire range of spatial and temporal frequencies that can be encoded by simple cells in the striate cortex.

To obtain a population response, we have taken an ensemble of the spatiotemporal amplitude spectra for all simple cells recorded from animals within the same age group.

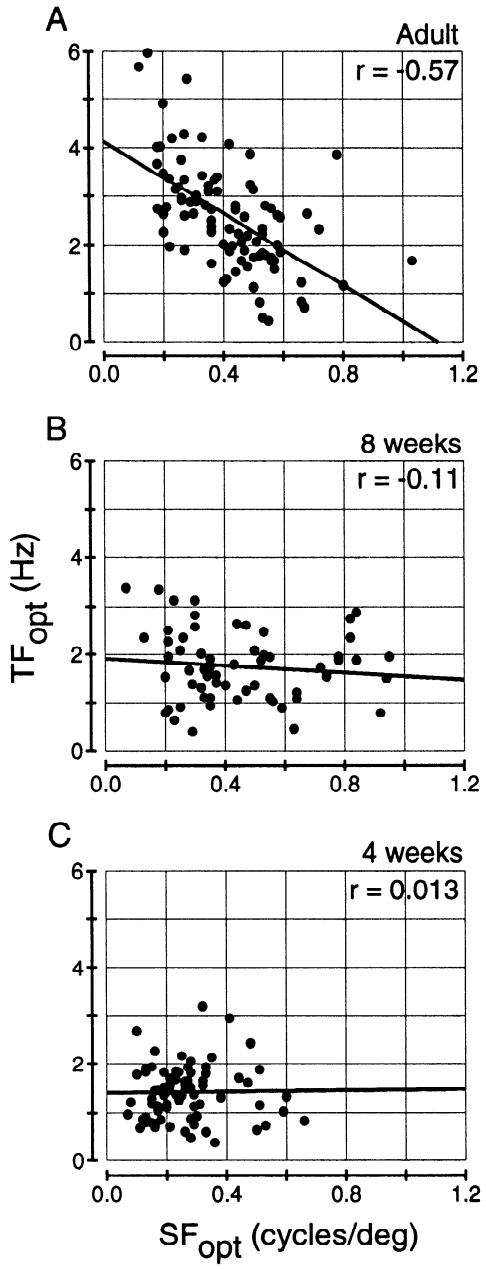

FIG. 14. Joint distribution of optimal spatial and temporal frequencies for populations of simple cells from adult cats (*A*), 8-wk-old kittens (*B*), and 4-wk-old kittens (*C*). In each panel, points are plotted at the coordinates determined by the values of SF_{opt} and TF_{opt} for each cell. Solid lines show the linear regression fit to each scatter of points. Note the significant negative correlation ($r = -0.57$) between TF_{opt} and SF_{opt} for cells from adults, and the lack of this negative correlation for kittens.

Specifically, the amplitude spectra of all cells are normalized and added together. The result of this operation is shown in Fig. 15*A* for the population ($n = 91$) of simple cells recorded from adult cats. The peak of this population response occurs at a spatial frequency of 0.36 cycles/deg and a temporal frequency of 2.6 Hz, and the response rolls off for higher and lower frequencies. This population response for adults is similar to that obtained by Baker (1990), with the use of drifting sinusoidal grating stimuli (see his Fig. 9).

Figure 15*B* shows the spatiotemporal population response for 8-wk-old kittens, and Fig. 15*C* shows the population response for 4-wk-old kittens. The peak response occurs at a spatial frequency of 0.37 cycles/deg and a temporal frequency of 1.7 Hz for 8-wk-old kittens, whereas the peak response for the population of cells from 4-wk-old kittens occurs at a spatial frequency of 0.23 cycles/deg and a temporal frequency of 1.4 Hz.

The difference in developmental time course between spatial frequency and temporal frequency tuning is evident in the population responses of Fig. 15. From 4 wk of age

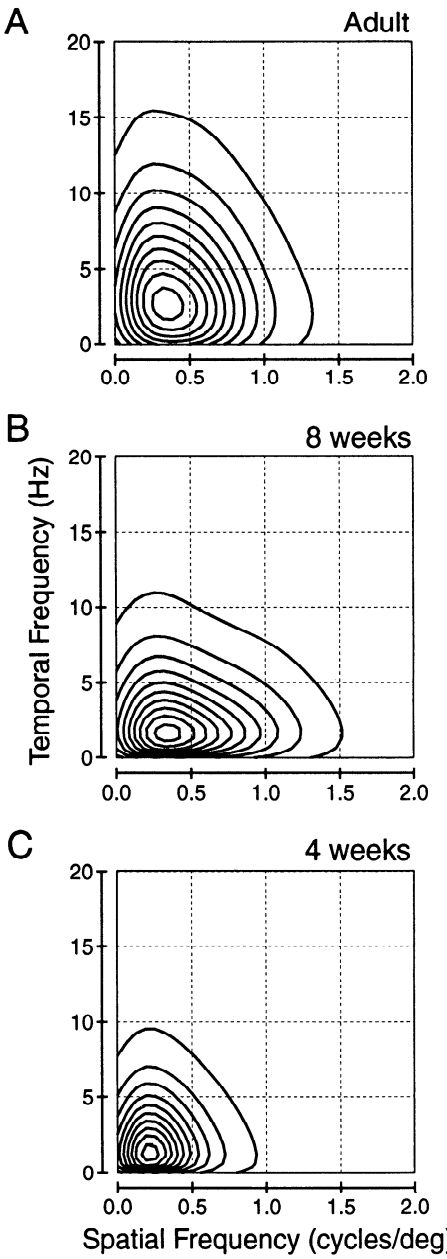

FIG. 15. Aggregate spatiotemporal frequency response for populations of simple cells from adult cats (*A*), 8-wk-old kittens (*B*), and 4-wk-old kittens (*C*). Each population response is obtained by adding together the spatiotemporal amplitude spectra (e.g., Fig. 11*B*) of all simple cells within a particular age group. Before summing these spectra, each is normalized to have a peak amplitude of 1.0. Each aggregate spatiotemporal frequency response is plotted as an isoamplitude contour map. Contours are plotted at 10 equally spaced amplitudes ranging from 5 to 95% of the peak value (in steps of 10%).

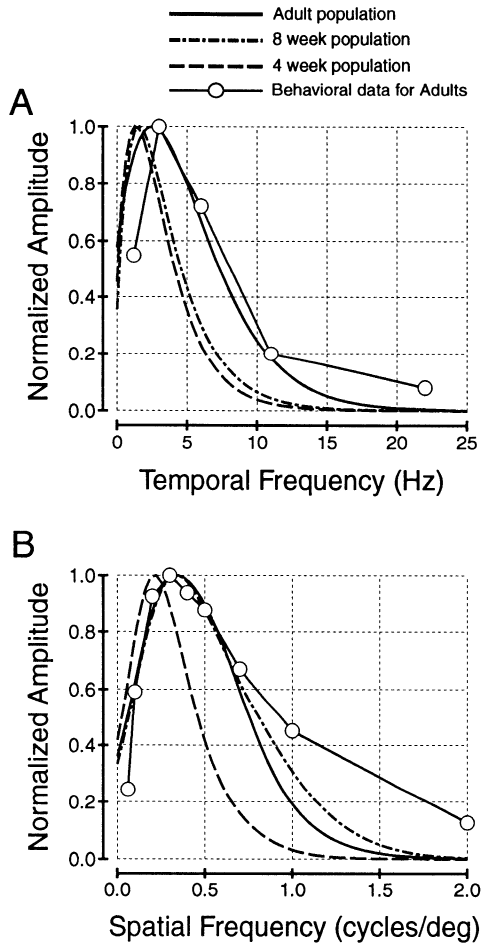

FIG. 16. Comparison of population response data with behavioral contrast sensitivity data. *A*: population response and behavioral data as a function of temporal frequency. Solid curve shows a cross section (parallel to the temporal frequency axis) through the peak of the population response for adults (Fig. 15*A*). Dashed and dot-dashed curves show temporal frequency cross sections of the population responses for 4-wk-old (Fig. 15*C*) and 8-wk-old (Fig. 15*B*) kittens, respectively. Open symbols (connected by solid lines) show behavioral contrast sensitivity data as a function of temporal frequency (reproduced from Blake and Camisa 1977). The contrast sensitivity data and population response cross sections have been normalized to a peak amplitude of 1.0 and plotted on the same scale. *B*: comparison of population response and behavioral data as a function of spatial frequency. Solid, dashed, and dot-dashed curves show spatial frequency cross sections through the population responses for adults, 8-wk kittens, and 4-wk kittens, respectively. Behavioral contrast sensitivity data as a function of spatial frequency (—○—) have been reproduced from Bisti and Maffei (1974). Data have been normalized to a peak value of 1.0.

(*C*) until 8 wk of age (*B*), there is a large increase in the range of spatial frequencies encoded by simple cells, but little change in the range of temporal frequencies that are encoded. From 8 wk of age until adulthood (*A*), the range of spatial frequencies that are encoded remains approximately constant, whereas the range of temporal frequencies increases substantially. These relationships are shown more quantitatively in Fig. 16. The solid curve in Fig. 16*A* is a temporal frequency cross section through the population response for adults, obtained by slicing (parallel to the temporal frequency axis) through the peak of the population response data. The dashed and dot-dashed lines in Fig. 16*A* show temporal frequency cross sections for 4- and 8-wk-old kittens, respectively. Figure 16*B* shows spatial frequency cross sections, obtained by slicing (parallel to the spatial frequency axis) through the peak of the population response, for each of the three age groups. Note that the spatial frequency cross section for 8-wk kittens is similar to that for adults (Fig. 16*B*), whereas the temporal frequency cross section for 8-wk-old kittens is similar to that for 4-wk-old kittens (Fig. 16*A*).

Figure 16 also shows a comparison of the population response data with behavioral contrast sensitivity data. If we assume that we have sampled a representative population of simple cells and that each cell contributes equally toward the detection of a stimulus, the population response should be somewhat similar in shape to a behavioral contrast sensitivity function. A comparison of the two types of data for adult cats suggests that these assumptions are not unreasonable. Figure 16*A* shows contrast sensitivity measured as a function of temporal frequency for an adult cat [○ (reproduced from Blake and Camisa 1977); spatial frequency was 0.5 cycles/deg]. The contrast sensitivity data are normalized to a peak value of 1.0 and plotted on the same scale as the temporal frequency cross section of the population response. Note that there is excellent agreement between the adult population response (solid curve) and the contrast sensitivity data (○), except at the lowest temporal frequency tested behaviorally (~1 Hz). This discrepancy at low frequencies may be explained by the fact that predicted temporal frequency tuning curves often exhibit less attenuation at low frequencies than tuning curves measured with gratings (see the companion paper). A similar comparison between the population response and behavioral data cannot be made for kittens, because, to our knowledge, contrast sensitivity data as a function of temporal frequency are not available.

Figure 16*B* shows a comparison between the spatial frequency cross section of the population response for adults (solid curve) and behavioral measurements of contrast sensitivity [○ (reproduced from Bisti and Maffei 1974)] as a function of spatial frequency. Again, both sets of data are normalized to have the same peak value (1.0). The behavioral data agree quite well with the population response, except for spatial frequencies above ~0.75 cycles/deg. The behavioral data show considerably less attenuation at high spatial frequencies (1–2 cycles/deg) than the population response. Thus the spatial acuity predicted by the population response is lower than that measured behaviorally. This discrepancy probably arises because we sample cells over a fairly large range of eccentricities (±15°). Alternatively, complex cells (which are not discussed here) might account for the difference between the population response and the behavioral data at high spatial frequencies. Nevertheless, the agreement between our population response and the behavioral data of Bisti and Maffei (1974) is surprisingly good, given the disparate nature of the two types of measurement. Our population response also agrees well with contrast sensitivity measurements obtained by Campbell et al. (1973) with the use of evoked potentials. It should be noted, however, that our population response peaks at a somewhat lower spatial frequency than the behavioral contrast sensitivity data obtained by Blake et al. (1974) and by Pasternak and Merigan (1981).

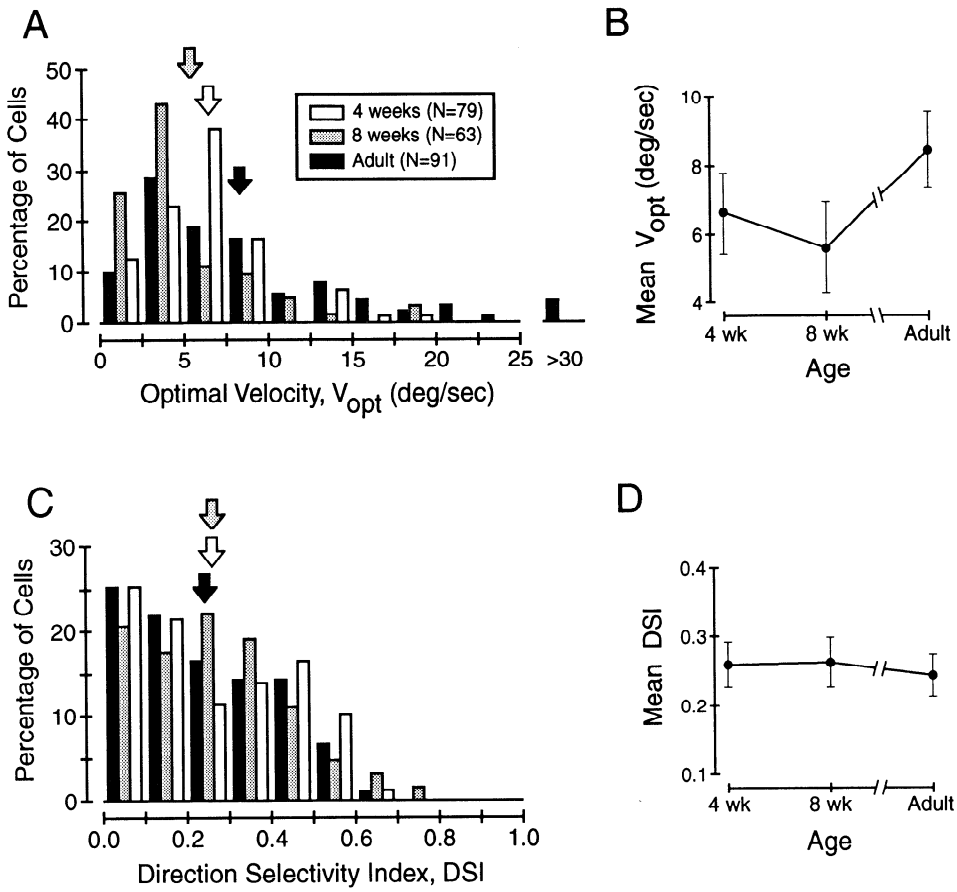

FIG. 17. Summary of changes in optimal velocity and direction selectivity as a function of age. *A*: distribution of optimal velocity (V_{opt}) for populations of simple cells from adults (■), 8-wk-old kittens (□), and 4-wk-old kittens (□). For each cell, V_{opt} is computed from the data of Figs. 12 and 13, with the use of *Eq. 6*. *B*: the mean value of V_{opt} is shown as a function of age. Error bars denote 95% confidence intervals. *C*: histogram showing the distribution of the direction selectivity index (DSI) for the same populations of simple cells as in *A*. The DSI is computed from the spatiotemporal amplitude spectrum for each cell, with the use of *Eq. 7*. *D*: mean DSI is plotted as a function of age. Note that there is no significant change in mean DSI with age.

Velocity and direction selectivity

Thus far we have used Fourier analysis of the X-T profile to characterize the spatial and temporal frequency selectivity of simple cells. In this section we show that this analysis can also be used to obtain estimates of a neuron's velocity tuning and direction selectivity.

For a linear spatiotemporal filter, the optimal velocity in response to a moving stimulus, V_{opt}, is simply the ratio of the optimal temporal frequency, TF_{opt}, and the optimal spatial frequency, SF_{opt}

$$V_{opt} = \frac{TF_{opt}}{SF_{opt}} \quad (6)$$

Recently, Baker (1990) has compared measurements of optimal velocity in response to moving bar stimuli with predictions of optimal velocity based on measurements of SF_{opt} and TF_{opt} obtained in response to drifting gratings. His study reveals a strong correlation ($r = 0.85$) between the measured and predicted values of V_{opt}. On the basis of this finding, we have computed optimal velocity from *Eq. 6*, with the use of values of SF_{opt} and TF_{opt} obtained via Fourier analysis of the X-T profile (as shown in Fig. 11). If we assume that our values of SF_{opt} and TF_{opt} are fairly accurate, as shown in the companion paper (DeAngelis et al. 1993), this computation yields reasonable estimates of optimal velocity.

Figure 17*A* shows the distribution of V_{opt} for simple cells from adult cats and kittens. The mean values are 8.4 deg/s for adults, 5.6 deg/s for 8-wk kittens, and 6.6 deg/s for 4-wk kittens. A one-way ANOVA shows a marginally significant effect of age on V_{opt} ($F_{2,230} = 4.06$, $P = 0.03$). It is interesting to note that the mean values of V_{opt} for 4-wk kittens and adult cats are not significantly different (Tukey's HSD test), although the distribution of V_{opt} is somewhat broader for adults. Apparently, the lower mean value of TF_{opt} in 4-wk-old kittens is compensated for by the lower mean value of SF_{opt}, such that the average V_{opt} does not change much. It should also be noted that the distribution of V_{opt} shown in Fig. 17*A* for adults is very similar to the distribution of optimal velocities reported by Baker (1990; see his Fig. 8*A*). Our distribution of V_{opt} is somewhat similar to that described by Movshon (1975) for simple cells, although he finds no simple cells tuned to velocities >8 deg/s. This difference may be attributable to the fact that we sample a larger range of eccentricities than Movshon did in his study; hence our mean value of SF_{opt} is lower.

In addition to determining optimal velocity, we can also extract estimates of direction selectivity from the 2-D amplitude spectra of simple cells. If the X-T profile of a linear spatiotemporal filter is oriented (i.e., space-time inseparable), then this filter will have a directional preference for motion (Adelson and Bergen 1985; Watson and Ahumada 1983, 1985). Equivalently, the spatiotemporal amplitude spectrum will be asymmetric along the temporal frequency axis. This can be seen clearly in Fig. 11, where the amplitude spectrum (*B*) has a much larger peak for positive temporal frequencies (corresponding to motion in the preferred direction) than for negative temporal frequencies (corresponding to motion in the nonpreferred direction). If we define the peak response amplitude for positive tem-

poral frequencies as R_p (denoting response in the *preferred* direction) and we define the peak amplitude for negative temporal frequencies as R_{np} (denoting response in the *nonpreferred* direction), then we can compute a DSI for the neuron as follows

$$\text{DSI} = \frac{R_p - R_{np}}{R_p + R_{np}} \quad (7)$$

For the cell of Fig. 11, the DSI has a value of 0.51 ($R_p = 213$, $R_{np} = 68$).

For cells with space-time separable receptive fields, the peaks in the spatiotemporal amplitude spectrum occur at approximately the same spatial and temporal frequencies for both directions of motion (and the peak amplitudes are approximately equal). However, for cells with inseparable X-T profiles, the peaks in the amplitude spectrum (e.g., Fig. 11) for the preferred and nonpreferred directions may occur at somewhat different spatial and temporal frequencies. In particular, when the X-T profile is inseparable, the peak temporal frequency in the nonpreferred direction tends to be higher than the peak temporal frequency in the preferred direction. A similar observation has been reported recently by Saul and Humphrey (1992), on the basis of responses to drifting sine-wave gratings.

Figure 17*C* shows the distribution of the DSI for populations of cells from adult cats, 8-wk-old kittens, and 4-wk-old kittens. Clearly, there is little difference between the distributions of DSI for these three age groups. Mean values are 0.24 for adults (➡), 0.26 for 8-wk-old kittens (⇛), and 0.26 for 4-wk-old kittens (⇨). There is no trend (ANOVA: $F_{2,230} = 0.29$, $P = 0.75$) for the DSI to change with age. Thus simple cells from kittens exhibit the same degree of direction selectivity (as measured by *Eq. 7*) as those from adults. This result is in agreement with previous findings (Albus and Wolf 1984; Bonds 1979; Braastad and Heggelund 1985; Pettigrew 1974).

It should be noted that the distribution of DSIs shown in Fig. 17*B* is *not* bimodal. Thus the spatiotemporal receptive fields of simple cells are not clearly divided into idealized separable and inseparable types, as conceptualized in theoretical descriptions (e.g., Adelson and Bergen 1985; Reid et al. 1991). Rather, there is a continuum of behavior from completely separable to strongly inseparable. Some cells are clearly intermediate between the idealized separable and inseparable types (see, for example, Fig. 2*A* of the companion paper, DeAngelis et al. 1993).

We have characterized the direction selectivity of simple cells by the degree of inseparability in their space-time receptive-field profiles. At this point, it is necessary to comment on how these estimates of direction selectivity compare with more traditional measurements obtained by the use of drifting sinusoidal gratings. This comparison is examined in detail in the companion paper (DeAngelis et al. 1993; see Figs. 9 and 10), where it is shown that the DSI determined from the amplitude spectrum accurately predicts the preferred direction of motion for virtually all cells. However, this predicted DSI typically underestimates the *strength* of the directional preference by about a factor of two. Thus there is some nonlinear process involved in the generation of direction selectivity. Similar conclusions have been reached by Reid et al. (1987, 1991), Tolhurst and Dean (1991), and Albrecht and Geisler (1991) by the use of different methods.

DISCUSSION

We have studied the spatiotemporal receptive-field structure of simple cells in the cat's striate cortex with the use of the reverse correlation technique (Jones and Palmer 1987a; McLean and Palmer 1989; Palmer et al. 1991). The advantage of this algorithm is that we can obtain estimates of a variety of response characteristics for simple cells, with the use of only a single test. Response latency and duration, receptive-field size and symmetry, spatial and temporal frequency selectivity, optimal velocity, and direction selectivity can all be assessed through measurement of a single X-T profile. This is advantageous for a developmental study because it is necessary to obtain, in a limited time, as much information as possible for each of a large number of cells. In this study we have focused exclusively on simple cells, because the reverse correlation algorithm of Fig. 2 is applicable in only a limited way to complex cells (see Palmer et al. 1991). For complex cells, spatial frequency (Movshon et al. 1978b; Szulborski and Palmer 1991), orientation (Szulborski and Palmer 1991), disparity (Ohzawa et al. 1990), and direction selectivity (Emerson et al. 1987) are probably determined by the structure of receptive-field *subunits* (see Szulborski and Palmer 1990) that are combined in some nonlinear fashion. The spatiotemporal organization of these subunits cannot be studied with the methods used here.[3] As a result, monocular receptive-field profiles from complex cells, as obtained by our method (see Fig. 1 of Ohzawa et al. 1990), do not provide much insight into the information-processing capabilities of these neurons.

The spatiotemporal structure of simple-cell receptive fields changes gradually over a period of several weeks after birth. Our data show that the spatial structure of simple cell receptive fields is mature at ~8 wk postnatal, whereas the temporal structure of these receptive fields matures considerably later. Thus the major finding of this study is that the developmental time courses of spatial and temporal properties are different in the striate cortex of cats. A similar conclusion has been drawn by Zumbroich et al. (1988) in their study of postnatal development in the lateral suprasylvian cortex of cats.

Spatiotemporal receptive-field structure of simple cells

Hubel and Wiesel (1959, 1962) initially described the receptive fields of simple cells as having spatially separate ON and OFF subregions. Illumination of an ON region with a small spot of light produces excitation at the onset of the stimulus, whereas an OFF region produces excitation when the spot of light is turned off. More recently, it has been shown (Ferster 1988) that an ON region produces excitation

[3] The receptive field profiles described here are essentially equivalent to a first-order kernel (e.g., Wiener 1958). To map the spatiotemporal structure of complex cell subunits, it is necessary to measure second-order kernels (see Emerson et al. 1987). Measurement of higher-order kernels requires a multi-input approach, in which more than one stimulus is presented to the neuron at a given time (e.g., Emerson et al. 1987; Movshon et al. 1978b; Szulborski and Palmer 1990).

in response to a bright stimulus and inhibition in response to a dark stimulus. Conversely, an OFF region produces excitation in response to a dark stimulus and inhibition in response to a bright stimulus. With this in mind, we have used the terms bright-excitatory and dark-excitatory to refer to ON and OFF subregions, respectively. Moreover, we have constructed composite receptive-field profiles (see Fig. 2*B*) by taking the difference between responses to bright and dark stimuli, as others have done previously (e.g., Jones and Palmer 1987a; Movshon et al. 1978a). The inherent assumption is that excitation produced by a dark stimulus is equivalent to inhibition produced by a bright stimulus, and vice versa. Because simple cells seldom exhibit any maintained discharge in the absence of a stimulus, it is not possible to directly measure the inhibitory effects produced by a bright or dark stimulus (without somehow artificially raising the cells' spontaneous firing) (see Palmer et al. 1991). On the basis of the observations of Ferster (1988), however, we can equate the inhibitory component of response to a bright stimulus with the excitatory component of response to a dark stimulus through subtraction (see the companion paper, as well as Palmer et al. 1991, for more on this point).

Following the qualitative observations of Hubel and Wiesel (1959, 1962), numerous researchers have made quantitative mappings of the receptive fields of simple cells. The most common method (Baker and Cynader 1986; Dean and Tolhurst 1983; DeValois et al. 1978; Field and Tolhurst 1986; Glezer et al. 1980, 1982; Heggelund 1981; Kulikowski and Bishop 1981; Maffei et al. 1979; Movshon et al. 1978a; Tadmor and Tolhurst 1989) is to construct a 1-D spatial receptive-field profile (or "line-weighting function") with the use of light and dark bars that are flashed on and off at various positions within the receptive field. It is generally assumed that a single spatial profile of this sort provides a functional description of the receptive field of a simple cell. However, this is only true, to some extent, for simple cells with space-time separable receptive fields. In these cases, the complete spatiotemporal receptive field, $R(X, T)$, is simply the product of a spatial profile, $G(X)$, and a temporal impulse response, $H(T)$ (see also Palmer et al. 1991). It is therefore possible to designate a particular spatial location within the receptive field as belonging to either a bright-excitatory or dark-excitatory subregion. It should be noted, however, that the temporal impulse response, $H(T)$, is typically biphasic, meaning that a subregion that exhibits an initial phase of excitation in response to a bright bar will usually show a second phase of excitation in response to a dark bar (e.g., Figs. 4*B* and 10*B*). This is most likely the origin of the "off" responses described by Hubel and Wiesel (1959, 1962). Another characteristic feature of simple cells with space-time separable receptive fields is that they possess a true "null" position (e.g., Albrecht and Geisler 1991; Reid et al. 1991). As defined by Enroth-Cugell and Robson (1966) in their study of ganglion cells, the null position (or null phase) is the location within the receptive field at which a counterphased grating stimulus produces no response, due to exact cancellation between ON and OFF regions.

For cells with space-time inseparable receptive fields, there is no unique spatial receptive-field profile. In these cases the bright- and dark-excitatory subregions move, within the receptive field, over time (see Fig. 4, *B, D,* and *F*) (see also McLean and Palmer 1989; Palmer et al. 1991). In other words, the spatial phase of the receptive field changes gradually as a function of time (see Fig. 10*G*). A consequence of this behavior is that inseparable receptive fields do not have a null position (Albrecht and Geisler 1991; Reid et al. 1991). Moreover, one cannot unambiguously designate a particular spatial location as belonging to either an ON or OFF subregion. This appears, at first glance, to violate Hubel and Wiesel's (1962) definition of a simple cell. However, the apparent contradiction is resolved when one views inseparable receptive fields in the joint space-time domain, where bright-excitatory (ON) and dark-excitatory (OFF) subregions are clearly segregated along an oblique axis (see Fig. 4, *B, D,* and *F*) (see also McLean and Palmer 1989).

It should be stressed that both spatial and temporal factors are important in characterizing the receptive fields of cortical cells. Conclusions drawn from spatial receptive-field profiles alone may be misleading. This point has often been overlooked in previous studies, in which spatial receptive-field profiles have been measured as line-weighting functions (Baker and Cynader 1986; Dean and Tolhurst 1983; DeValois et al. 1978; Field and Tolhurst 1986; Glezer et al. 1980, 1982; Heggelund 1981; Kulikowski and Bishop 1981; Maffei et al. 1979; Movshon et al. 1978a; Tadmor and Tolhurst 1989). Although the methodology for constructing these profiles varies somewhat from study to study, the response at a given position is generally determined by accumulating the responses (i.e., counting spikes) elicited by the stimulus over some period of time. This is tantamount to performing a temporal integration. Consider, for example, the effects of this temporal integration on the measurement of receptive-field phase. As noted above, spatial phase changes over time for cells with inseparable X-T profiles. For these cells, the spatial phase of the line-weighting function probably reflects a time average of the actual time-varying phase. This value of spatial phase may therefore depend on the conditions of stimulation and the particular method used to accumulate responses over time. Only for space-time separable receptive fields would the phase of the line-weighting function be a unique characteristic of the neuron (see also Hamilton et al. 1989 on this point). Hence some previous data (Field and Tolhurst 1986; Hamilton et al. 1989) showing the distribution of spatial phases for simple receptive fields may be misleading.

Development of spatial receptive-field structure

Our data reveal that the spatiotemporal receptive-field structure of simple cells in kittens is qualitatively very similar to that of cells from adult cats (see Fig. 4). Like those from adults, the receptive fields of most cells from kittens have at least two or three spatially segregated bright- and dark-excitatory (ON and OFF) subregions (see Fig. 8*E*). This agrees with the findings of Braastad and Heggelund (1985), who found simple cells to have both ON and OFF subregions even in very young kittens (1–2 wk old). Hubel and Wiesel (1963) also noted that many cells in kittens 1–3 wk old show receptive fields that would be classified as sim-

ple on the basis of the criteria outlined for adult cats. Our findings (Fig. 8*E*) appear to conflict, however, with those of Albus and Wolf (1984), who report that 60% of visually responsive neurons from kittens 20–24 days old have unimodal receptive fields, consisting of only a single ON or OFF subregion. We did encounter some (7/79 = 8.8%) unimodal receptive fields in our population of simple cells from 28-day-old kittens, but the proportion is not substantially larger than the number of unimodal receptive fields encountered in adults (6/91 = 6.6%). Perhaps the difference between our results and those of Albus and Wolf (1984) is due to the greater sensitivity of the reverse correlation method for mapping receptive fields. It should be noted, however, that we have no data from kittens younger than 28 days of age. Nevertheless, it seems unlikely that the proportion of unimodal cells could decrease from 60 to 8.8% in just a few days.

Although we find that the receptive fields of simple cells in kittens are qualitatively similar to those in adults, there are important quantitative differences between animals of different ages. Let us first consider spatial parameters of receptive-field structure. The data of Fig. 13 show that spatial frequency selectivity becomes finer with age until ~8 wk postnatal. There is essentially no difference in spatial frequency selectivity between populations of simple cells from 8-wk-old kittens and adult cats. These results agree reasonably well with the findings of Derrington and Fuchs (1981), who measured spatial frequency selectivity with the use of sinusoidal gratings. Our data are also consistent with those of Braastad and Heggelund (1985), who measured the width of the dominant receptive-field subregion as a function of age. For simple cells, the width of this subregion is inversely related to the cell's optimal spatial frequency. Braastad and Heggelund (1985) show that subregion size decreases substantially for kittens between 4 and 8 wk postnatal, whereas the average subregion width of 8-wk-old kittens is comparable with that for adult cats.

It is likely that the increase in spatial resolution of simple cells as a function of age results from developmental changes that occur subcortically. The width of the dominant subregion of simple cells decreases with age (see Fig. 1 of Braastad and Heggelund 1985) at almost exactly the same rate as the receptive-field center size of retinal ganglion cells (Rusoff and Dubin 1977). Moreover, the preferred spatial frequency for neurons in the kitten's lateral geniculate nucleus (LGN) matures with a similar time course to the optimal spatial frequency of cells in the cortex (Ikeda and Tremain 1978).

Another point worth noting is that the spatial symmetry (or phase) of simple-cell receptive fields is uniformly distributed for both kittens and cats (see Fig. 9). Thus, although the size of the receptive fields and the preferred spatial frequency change with age, simple cells appear to always exhibit a variety of symmetries. This is true regardless of whether one considers all simple cells or just those that have space-time separable receptive fields.

Development of temporal selectivity

Let us now consider the postnatal development of temporal receptive-field characteristics. A central finding of this study is that the time course of development is different for spatial and temporal aspects of receptive-field structure. Although spatial structure appears mature by 8 wk of age, temporal structure continues to develop well past 8 wk postnatal (see Figs. 5, 7, and 12). A similar finding has been reported by Zumbroich et al. (1988), who show that the spatial frequency selectivity of cells in the lateral suprasylvian cortex matures earlier than the temporal frequency selectivity. To our knowledge, there are no other data available on the relative rates of development of spatial and temporal selectivity in the visual cortex.

Because the postnatal development of temporal selectivity has received much less attention than the development of spatial selectivity, it is not clear whether temporal development depends mainly on central or peripheral factors. There is some evidence, however, that the temporal response properties of cortical cells are limited by development of the retina. Hamasaki and Flynn (1977) report that the average response latency of ganglion cells in 3-wk-old kittens is 1.8 times longer than the mean latency of responses from adults. By comparison, we find that the mean latency for simple cells from 4-wk-old kittens is 1.67 times that for cells from adults (see Fig. 5*C*). Moreover, Flynn et al. (1977) show that the distribution of response latencies for ganglion cells does not become mature until 12 wk of age. Flynn et al. also find that the response of ganglion cells to stimuli of different temporal frequencies does not mature until ~20 wk postnatal. Our data are insufficient to determine exactly when the temporal response characteristics of simple cells reach maturity, but they are consistent with the findings of Flynn et al. (1977).

It is also possible that the development of temporal selectivity in the striate cortex depends on changes that occur upstream from the retina. Myelination of the cat's optic tract progresses rapidly between the second and fourth postnatal weeks but does not reach completion until 12 wk of age (Moore et al. 1976). Myelination of fibers in the visual cortex begins during the fifth postnatal week and continues well beyond the age of 20 wk (Haug et al. 1976). Tsumoto and Suda (1982) have shown that latencies of cortical cells in response to electrical stimulation at the LGN decrease with age until ~6–8 wk postnatal. In addition, they report that the synaptic delay for cortical cells driven monosynaptically from the LGN declines sharply with age, reaching adult values by ~12 wk postnatal. It is also worth noting that the density of synapses in the visual cortex reaches a peak near 7 wk of age and declines somewhat thereafter (Cragg 1975). Recently, Hestrin (1992) has reported that the duration of *N*-methyl-D-aspartate (NMDA) receptor–mediated postsynaptic currents decreases severalfold during postnatal development of the superior colliculus. A similar mechanism could contribute to the maturation of temporal response properties in the visual cortex. Thus, although the maturation of temporal selectivity in cortical cells is clearly limited by the development of the retina (Flynn et al. 1977), there are several other factors that may contribute to the temporal immaturity of simple cells that we have observed. Further studies will be necessary to establish which of these extraretinal factors play a significant role in the maturation of temporal receptive-field structure.

Although the factors that determine the development of

temporal selectivity are not completely understood, our data place an important constraint on these developmental mechanisms. Figure 14 shows clearly that the increase in mean optimal temporal frequency with age depends on spatial frequency. Cells tuned to low spatial frequencies exhibit a large increase in TF_{opt} between 8 wk of age and adulthood, whereas cells tuned to high spatial frequencies do not. Thus temporal maturation (beyond 4 wk postnatal) is a selective process, involving mainly cells tuned to low spatial frequencies. This cannot be explained by developmental factors such as myelination of fibers, because this should affect all cells. One possible explanation for this finding is that there are two sets of inputs to a given population of simple cells that carry low and high spatial frequency information, respectively. If so, then it is plausible that the low spatial frequency inputs undergo some temporal maturation process after 8 wk postnatal, whereas the high spatial frequency inputs do not. It is tempting to speculate that simple cells tuned to low and high spatial frequencies might receive input from Y- and X-cells, respectively, of the LGN, because X-cells tend to prefer higher spatial frequencies than Y-cells (e.g., Derrington and Fuchs 1979). Consistent with this idea, Mangel et al. (1983) report that the temporal resolution of LGN Y-cells increases considerably beyond 8 wk postnatal, whereas the temporal resolution of X-cells is nearly mature at 8 wk of age. However, the experimental evidence concerning synaptic inputs to striate cortex from X- and Y-cells does not clearly support this speculation. Several studies have concluded that both X- and Y-cells of the LGN project to the striate cortex (see Gilbert 1983; Lennie 1980; Martin 1984 for reviews). In fact, some studies (Ferster and LeVay 1978; Gilbert and Wiesel 1979; Henry et al. 1979) report that X- and Y-type afferents to the striate cortex are segregated into different sublaminae of layer 4. However, some more recent studies, employing both intracellular and extracellular recording techniques, suggest that X- and Y-cell inputs are segregated into areas 17 and 18, respectively (Ferster 1990a,b). Moreover, Ferster and Jagadeesh (1991) have recently shown that simple cells in area 17 rarely exhibit a Y-type nonlinearity, whereas many simple cells in area 18 exhibit this form of nonlinearity. Thus it is difficult to conclude whether our findings on the development of temporal frequency selectivity may be related to parallel inputs from X- and Y-cells.

Possible sources of error

Our findings are based on the analysis of spatiotemporal receptive-field profiles obtained with the use of the reverse correlation technique (Jones and Palmer 1987a; McLean and Palmer 1989; Palmer et al. 1991). Because this method is relatively new to visual neurophysiology, it is important to consider some of the possible sources of error that may be inherent in our measurements. One general observation is that cells that respond poorly (<5 spikes/s) to drifting sinusoidal gratings do not usually yield receptive-field profiles with an adequate signal-to-noise ratio, unless one collects data over a very long time period. Most simple cells from adult cats are responsive enough to yield smooth receptive-field profiles in a period of 20–30 min, but this is not always the case for cells from young kittens. It is well documented that the responsivity of striate neurons increases considerably over the first several weeks of postnatal life (e.g., Albus and Wolf 1984; Bonds 1979; Braastad and Heggelund 1985; Freeman and Ohzawa 1992). Not surprisingly, we often encounter simple cells in 4-wk-old kittens that respond sluggishly to the visual stimulus during reverse correlation analysis. As a result, our population of neurons from 4-wk-old kittens (and, to a lesser extent, that from 8-wk-old kittens) is somewhat biased in favor of more responsive cells. This means that we might be *underestimating* the overall magnitude of spatial and temporal differences between 4-wk-old kittens and adult cats, because the more responsive cells would also tend to be more mature. In many cases, cells from kittens do not give a vigorous response when the full 2-D reverse correlation stimulus ensemble is used, but produce reasonable results with the 1-D stimulus (see METHODS).

In addition to responsivity, there are several other sources of error that could affect the data reported here. Because we have used Fourier analysis to obtain estimates of spatial and temporal frequency tuning from X-T profiles, our data are obviously prone to error if simple cells exhibit nonlinear spatial and temporal summation. The companion paper (DeAngelis et al. 1993) addresses this issue in detail and reveals that response nonlinearities do not affect our main findings (at least for the parameters we have used to gauge frequency selectivity in this paper).

Nevertheless, there are still potential sources of error to be aware of, even if simple cells behave linearly. Let us first consider sources of error pertinent to the spatial dimension of our data. One potential problem is blurring of the receptive-field profile due to the size (width) of the reverse correlation bar stimulus. If the width of the bar becomes a substantial fraction of the width of a receptive-field subregion, the receptive-field profile will be smoothed, or blurred. This is tantamount to attenuating high spatial frequency components in the data. This sort of blurring can lead to erroneous (too low) estimates of the optimal spatial frequency and high spatial frequency cutoff, when these are obtained through Fourier analysis. Fortunately, it is a simple computation to determine whether or not the size of the stimulus has a significant effect on the spectral content of the data (see APPENDIX). A few cells have been discarded from our sample because of significant blurring due to stimulus width. For all other cells, the effect of blurring on the spatial frequency estimates (SF_{opt} and SF_{high}) is very small (<5% on average). It is important to note that errors due to blurring mainly affect cells in our sample that are tuned to high spatial frequencies (i.e., some of those from 8-wk-old kittens and adults). As a result, this type of error would tend to *reduce* the differences between 4-wk-old kittens and adult cats shown in Fig. 13.

Another potential source of error in spatial receptive-field profiles arises from errors in determination of the cells' preferred orientation. If the orientation of the stimulus grid and bar stimuli (see Fig. 2*A*) does not closely match the preferred orientation of the receptive field, then integration of the 2-D spatial profile along the Y-axis (see Fig. 3) can produce some distortion of the X-T profile. This type of error is negligible for most of the cells in this study because the preferred orientation was determined quantitatively

with gratings. In addition, a curve-fitting procedure was applied to the orientation tuning curves to aid in extracting the optimal orientation to within a degree or two. For a couple of cells, there was a significant orientation misalignment between the stimulus grid and the receptive field; these cells were omitted from further analysis.

A potential source of error in the distributions of spatial frequency parameters shown in Fig. 13 involves the range of receptive-field eccentricities sampled in each age group. Because receptive-field size increases and optimal spatial frequency decreases with eccentricity (see Movshon et al. 1978c), the distribution of spatial frequency parameters depends on the range of eccentricities sampled. Thus it is conceivable that the differences between age groups seen in Fig. 13 is an artifact of some sampling bias for eccentricity. We feel strongly, however, that this is unlikely. In all animals, we made long (4–5 mm) penetrations down the medial bank of the postlateral gyrus. Because of the consistency of the penetrations, we generally encountered a similar range of receptive-field eccentricities (±15°) in all animals, so that there appears to be no overt sampling bias for eccentricity.

Finally, let's consider sources of error that affect the temporal dimension of our data. As for the spatial dimension, one possible source of error is blurring due to the duration of the reverse correlation stimulus. If the stimulus duration is too long, high temporal frequency components may be filtered out of the data, and estimates of TF_{opt} and TF_{high} may be erroneously low. In the earliest experiments we used a standard stimulus duration of 52 ms (4 refresh cycles on our display); in later experiments we have adjusted the duration on the basis of measured temporal frequency tuning curves (by subtracting or adding multiples of 13 ms). For a few cells the stimulus duration was too long, and temporal frequencies within the cell's bandwidth were attenuated significantly (see APPENDIX); these cells were omitted from the sample. For all other cells, the effect of stimulus duration on the estimated temporal frequency tuning curves is minimal (3–4% on average). Moreover, blurring errors due to stimulus duration only affect cells in our sample that are tuned to high temporal frequencies (i.e., some of those from adult cats). This error would, therefore, tend to reduce the differences between adults and kittens shown in Fig. 12.

Another potential source of error concerns the dependence of temporal selectivity on luminance. It is known that the temporal response properties of cortical cells can change as mean luminance is decreased (see Carney et al. 1989; Kaufman and Palmer 1990). With the use of the reverse correlation technique, Kaufman and Palmer (1990) have shown that the temporal structure of simple receptive fields changes considerably as luminance decreases, whereas the spatial structure is largely unaffected. They report that response latency and receptive-field duration increase at luminances below 1–2 cd/m^2, whereas the optimal temporal frequency and high temporal frequency cutoff decrease. These differences at low luminances are similar to the differences we have observed between kittens and cats. Thus it is conceivable that the developmental changes we have observed reflect some difference in the luminance dependence of receptive-field structure between kittens and cats. If so, then the temporal immaturity of cells from kittens might be reduced, or even disappear, if tested at a higher mean luminance.

To evaluate this possibility, we have obtained repeat measurements of the X-T profile at different luminances for several cells from kittens and cats. Most of the data in this study were obtained at an effective luminance of 6 cd/m^2. However, for several cells ($n = 7$), we replaced the beam splitters shown in Fig. 1 with full-silvered mirrors, so that the effective mean luminance at the cat's eye increased to ~35 cd/m^2. In no case did we find a significant change with luminance in any of the temporal response parameters we have measured. Therefore we conclude that the differences in temporal selectivity between kittens and cats are maintained at higher luminances.

In summary, we have provided a detailed quantitative description of the spatiotemporal receptive fields of simple cells in the striate cortex. From these measurements we conclude that spatial selectivity matures considerably earlier than temporal selectivity. In the companion paper (DeAngelis et al. 1993), we evaluate the predictive power of a linear spatiotemporal filter model for simple cells.

APPENDIX

We would like the X-T profile of a simple cell to approximate the spatiotemporal impulse response of that neuron. Hence we need the stimulus to approximate an impulse. A spatiotemporal impulse, formally defined, has infinite amplitude and infinitesimal dimensions in both space and time, such that the total volume under the function is equal to one. For our purposes, it is not possible to generate such a stimulus, nor will a cell respond to a stimulus of finite magnitude having infinitesimal dimensions. Thus we must try to approximate an impulse while providing a reasonably potent stimulus.

In the frequency domain, the amplitude spectrum of an impulse is constant across all frequencies (i.e., the spectrum is white). On the other hand, most neurons are tuned to a fairly small range of spatial and temporal frequencies. If the amplitude spectrum of our stimulus is approximately flat over the range of frequencies to which a neuron responds, then the stimulus will be an adequate approximation to an impulse. For simplicity, let us consider our stimulus as a function of time and one dimension of space, keeping in mind that the following computations easily generalize to two dimensions of space.

The stimulus in our reverse correlation experiments, $S(x, t)$, is a square pulse in both space (x) and time (t). The amplitude spectrum of this stimulus, $S(u, v)$, is a 2-D sinc function in spatiotemporal frequency space. If the reverse correlation bar stimulus has a width of Δx degrees and a duration of Δt seconds, then the first zero crossings of the 2-D sinc function will occur at a spatial frequency of $u = 1/\Delta x$ cycles/deg and a temporal frequency of $v = 1/\Delta t$ Hz. For spatial and temporal frequencies below approximately $u = 1/3\Delta x$ and $v = 1/3\Delta t$, respectively, $S(u, v)$ is fairly flat, and $S(x, t)$ will be a good approximation to an impulse. For spatial and temporal frequencies above about $u = 1/2\Delta x$ and $v = 1/2\Delta t$, respectively, the rolloff of $S(u, v)$ starts to become substantial.

In this study we have measured the spatiotemporal amplitude spectrum, $M(u, v)$, of individual simple cells. Because our stimulus is not actually an impulse, the measured amplitude spectrum, $M(u, v)$, for a cell is actually the product of the amplitude spectrum of the stimulus, $S(u, v)$, and the true frequency spectrum, $F(u, v)$, of the neuron

$$M(u, v) = S(u, v) \times F(u, v)$$

Thus we can estimate the true amplitude spectrum of the neuron, $F(u, v)$, as

$$F(u, v) = \frac{M(u, v)}{S(u, v)}$$

If our stimulus is a reasonable approximation to an impulse, then $S(u, v)$ will be approximately equal to one over the range of spatial and temporal frequencies for which $M(u, v)$ is nonzero. Consequently, $M(u, v)$ will be a close approximation to $F(u, v)$. In practice, we have computed $F(u, v)$ and extracted values of SF_{opt}, TF_{opt}, SF_{high}, and TF_{high}. These values are then compared with the values obtained directly from the measured spectrum, $M(u, v)$. If the two sets of values differ by no more than a few percent, we conclude that the blurring effect of our stimulus has not had a significant impact on our measurements.

We are grateful to G. Ghose for participating in these experiments and for many helpful comments.

This work was supported by research and CORE grants from the National Eye Institute (EY-01175 and EY-03176) and by a collaborative project of the Human Frontier Science Program.

Address for reprint requests: R. D. Freeman, School of Optometry, 360 Minor Hall, University of California, Berkeley, Berkeley, CA 94720.

Received 3 August 1992; accepted in final form 17 November 1992.

REFERENCES

ADELSON, E. H. AND BERGEN, J. R. Spatio-temporal energy models for the perception of motion. *J. Opt. Soc. Am. A* 2: 284–299, 1985.

ALBRECHT, D. G. AND GEISLER, W. S. Motion selectivity and the contrast-response function of simple cells in the visual cortex. *Visual Neurosci.* 7: 531–546, 1991.

ALBUS, K. AND WOLF, W. Early post-natal development of neuronal function in the kitten's visual cortex: a laminar analysis. *J. Physiol. Lond.* 348: 153–185, 1984.

BAKER, C. L. Spatial- and temporal-frequency selectivity as a basis for velocity preference in cat striate cortex neurons. *Visual Neurosci.* 4: 101–113, 1990.

BAKER, C. L. AND CYNADER, M. S. Spatial receptive-field properties of direction-selective neurons in cat striate cortex. *J. Neurophysiol.* 55: 1136–1152, 1986.

BARLOW, H. B. AND PETTIGREW, J. D. Lack of specificity in neurones in the visual cortex of young kittens (Abstract). *J. Physiol. Lond.* 218: 98P–101P, 1971.

BISTI, S. AND MAFFEI, L. Behavioural contrast sensitivity of the cat in various visual meridians. *J. Physiol. Lond.* 241: 201–210, 1974.

BLAKE, R. AND CAMISA, J. M. Temporal aspects of spatial vision in the cat. *Exp. Brain Res.* 28: 325–333, 1977.

BLAKE, R., COOL, S. J., AND CRAWFORD, M. L. J. Visual resolution in the cat. *Vision Res.* 14: 1211–1217, 1974.

BLAKEMORE, C. AND VAN SLUYTERS, R. C. Innate and environmental factors in the development of the kitten's visual cortex. *J. Physiol. Lond.* 248: 663–716, 1975.

BONDS, A. B. Development of orientation tuning in the visual cortex of kittens. In: *Developmental Neurobiology of Vision,* edited by R. D. Freeman. New York: Plenum, 1979, p. 31–41.

BRAASTAD, B. O. AND HEGGELUND, P. Development of spatial receptive-field organization and orientation selectivity in kitten striate cortex. *J. Neurophysiol.* 53: 1158–1178, 1985.

BRACEWELL, R. N. *The Fourier Transform and Its Applications* (2nd ed.). New York: McGraw-Hill, 1978.

BUISSERET, P. AND IMBERT, M. Visual cortical cells: their developmental properties in normal and dark-reared kittens. *J. Physiol. Lond.* 255: 511–525, 1976.

CAMPBELL, F. W., MAFFEI, L., AND PICCOLINO, M. The contrast sensitivity of the cat. *J. Physiol. Lond.* 229: 719–731, 1973.

CARNEY, T., PARADISO, M. A., AND FREEMAN, R. D. A physiological correlate of the Pulfrich effect in cortical neurons of the cat. *Vision Res.* 29: 155–165, 1989.

COOPER, G. F. AND ROBSON, J. G. Successive transformations of spatial information in the visual system. *IEE Natl. Physiol. Lab. Conf. Proc.* 42: 134–143, 1968.

CRAGG, B. G. The development of synapses in the visual system of the cat. *J. Comp. Neurol.* 160: 147–166, 1975.

DEAN, A. F. AND TOLHURST, D. J. On the distinctiveness of simple and complex cells in the visual cortex of the cat. *J. Physiol. Lond.* 344: 305–325, 1983.

DEANGELIS, G. C., GHOSE, G. M., OHZAWA, I., AND FREEMAN, R. D. Spatiotemporal receptive field structure and phase relationships between adjacent simple cells in the cat's striate cortex. *Soc. Neurosci. Abstr.* 18: 10, 1992.

DEANGELIS, G. C., OHZAWA, I., AND FREEMAN, R. D. Depth is encoded in the visual cortex by a specialized receptive field structure. *Nature Lond.* 352: 156–159, 1991.

DEANGELIS, G. C., OHZAWA, I., AND FREEMAN, R. D. Spatiotemporal organization of simple-cell receptive fields in the cat's striate cortex. II. Linearity of temporal and spatial summation. *J. Neurophysiol.* 69: 1118–1135, 1993.

DEANGELIS, G. C., OHZAWA, I., FREEMAN, R. D., AND GHOSE, G. M. Properties of length and width tuning of cells in the cat's striate cortex (Abstract). *Invest. Ophthalmol. Visual Sci. Suppl.* 31: 430, 1990.

DEBOER, E. AND KUYPER, P. Triggered correlation. *IEEE Trans. Biomed. Eng.* 15: 169–179, 1968.

DERRINGTON, A. M. AND FUCHS, A. F. Spatial and temporal properties of X and Y cells in the cat lateral geniculate nucleus. *J. Physiol. Lond.* 293: 347–364, 1979.

DERRINGTON, A. M. AND FUCHS, A. F. The development of spatial-frequency selectivity in kitten striate cortex. *J. Physiol. Lond.* 316: 1–10, 1981.

DEVALOIS, R. L., ALBRECHT, D. G., AND THORELL, L. G. Cortical cells: bar and edge detectors or spatial-frequency analyzers? In: *Frontiers in Visual Science,* edited by S. J. Cool and E. L. Smith. New York: Springer-Verlag, 1978, p. 544–556.

EGGERMONT, J. J., JOHANNESMA, P. I. M., AND AERTSEN, A. M. H. J. Reverse-correlation methods in auditory research. *Q. Rev. Biophys.* 16: 341–414, 1983.

EMERSON, R. C., CITRON, M. C., VAUGHN, W. J., AND KLEIN, S. A. Nonlinear directionally selective subunits in complex cells of cat striate cortex. *J. Neurophysiol.* 58: 33–65, 1987.

ENROTH-CUGELL, C. AND ROBSON, J. G. The contrast sensitivity of retinal ganglion cells of the cat. *J. Physiol. Lond.* 187: 517–552, 1966.

FERSTER, D. Spatially opponent excitation and inhibition in simple cells of the cat visual cortex. *J. Neurosci.* 8: 1172–1180, 1988.

FERSTER, D. X- and Y-mediated synaptic potentials in neurons of areas 17 and 18 of cat visual cortex. *Visual Neurosci.* 4: 115–133, 1990a.

FERSTER, D. X- and Y-mediated current sources in areas 17 and 18 of cat visual cortex. *Visual Neurosci.* 4: 135–145, 1990b.

FERSTER, D. AND JAGADEESH, B. Nonlinearity of spatial summation in simple cells of areas 17 and 18 of cat visual cortex. *J. Neurophysiol.* 66: 1667–1679, 1991.

FERSTER, D. AND LEVAY, S. The axonal arborization of lateral geniculate neurons in the striate cortex of the cat. *J. Comp. Neurol.* 182: 923–944, 1978.

FIELD, D. J. AND TOLHURST, D. J. The structure and symmetry of simple-cell receptive-field profiles in the cat's visual cortex. *Proc. R. Soc. Lond. B Biol. Sci.* 228: 379–400, 1986.

FLYNN, J. T., FLYNN, T. E., HAMASAKI, D. I., NAVARRO, O., SUTIJA, V. G., AND TUCKER, G. S. Development of the eye and retina of kittens. In: *Frontiers in Visual Science,* edited by S. J. Cool and E. L. Smith III. New York: Springer-Verlag, p. 594–603, 1977.

FREEMAN, R. D. AND OHZAWA, I. Monocularly deprived cats: binocular tests of cortical cells reveal functional connections from the deprived eye. *J. Neurosci.* 8: 2491–2506, 1988.

FREEMAN, R. D. AND OHZAWA, I. On the neurophysiological organization of binocular vision. *Vision Res.* 30: 1661–1676, 1990.

FREEMAN, R. D. AND OHZAWA, I. Development of binocular vision in the kitten's striate cortex. *J. Neurosci.* 12:4721–4736, 1992.

FREGNAC, Y. AND IMBERT, M. Early development of visual cortical cells in normal and dark-reared kittens: relationship between orientation selectivity and ocular dominance. *J. Physiol. Lond.* 278: 27–44, 1978.

FREGNAC, Y. AND IMBERT, M. Development of neuronal selectivity in primary visual cortex of cat. *Physiol. Rev.* 64: 325–434, 1984.

GABOR, D. Theory of communication. *J. Inst. Electr. Eng.* 93: 429–457, 1946.

GHOSE, G. M., OHZAWA, I., AND FREEMAN, R. D. Cross-correlation analysis of intracortical synaptic plasticity in kittens (Abstract). *Invest. Ophthalmol. Visual Sci. Suppl.* 31: 7, 1990.

GHOSE, G. M., OHZAWA, I., AND FREEMAN, R. D. Stimulus dependent correlated discharge in the cat's visual cortex (Abstract). *Invest. Ophthalmol. Visual Sci. Suppl.* 32: 908, 1991.

GILBERT, C. D. Microcircuitry of the visual cortex. *Annu. Rev. Neurosci.* 6: 217–247, 1983.

GILBERT, C. D. AND WIESEL, T. N. Morphology and intracortical projections of functionally identified neurons in cat visual cortex. *Nature Lond.* 280: 120–125, 1979.

GLEZER, V. D., TSCHERBACH, T. A., GAUSELMAN, V. E., AND BONDARKO, V. M. Linear and nonlinear properties of simple and complex receptive fields in area 17 of the cat visual cortex. *Biol. Cybern.* 37: 195–208, 1980.

GLEZER, V. D., TSCHERBACH, T. A., GAUSELMAN, V. E., AND BONDARKO, V. M. Spatio-temporal organization of receptive fields of the cat's striate cortex. *Biol. Cybern.* 43: 35–49, 1982.

HAMASAKI, D. I. AND FLYNN, J. T. Physiological properties of retinal ganglion cells of 3-week-old kittens. *Vision Res.* 17: 275–284, 1977.

HAMILTON, D. B., ALBRECHT, D. G., AND GEISLER, W. S. Visual cortical receptive fields in monkey and cat: spatial and temporal phase transfer function. *Vision Res.* 29: 1285–1308, 1989.

HAUG, H., KOLLN, M. AND RAST, A. The postnatal development of myelinated nerve fibers in the visual cortex of the cat. A stereological and electron microscopical investigation. *Cell Tissue Res.* 167: 265–288, 1976.

HEGGELUND, P. Receptive field organization of simple cells in cat striate cortex. *Exp. Brain Res.* 42: 89–98, 1981.

HEGGELUND, P. Quantitative studies of the discharge fields of single cells in cat striate cortex. *J. Physiol. Lond.* 373: 277–292, 1986.

HENRY, G. H., HARVEY, A. R., AND LUND, J. S. The afferent connections and laminar distribution of cells in the cat striate cortex. *J. Comp. Neurol.* 187: 725–744, 1979.

HESTRIN, S. Developmental regulation of NMDA receptor–mediated synaptic currents at a central synapse. *Nature Lond.* 357: 686–689, 1992.

HOLUB, R. A. AND MORTON-GIBSON, M. Response of visual cortical neurons of the cat to moving sinusoidal gratings: response-contrast functions and spatiotemporal interactions. *J. Neurophysiol.* 46: 1244–1259, 1981.

HUBEL, D. H. AND WIESEL, T. N. Receptive fields of single neurones in the cat's striate cortex. *J. Physiol. Lond.* 148: 574–591, 1959.

HUBEL, D. H. AND WIESEL, T. N. Receptive fields, binocular interaction and functional architecture in the cat's visual cortex. *J. Physiol. Lond.* 160: 106–154, 1962.

HUBEL, D. H. AND WIESEL, T. N. Receptive fields of cells in striate cortex of very young, visually inexperienced kittens. *J. Neurophysiol.* 26: 994–1002, 1963.

IKEDA, H. AND TREMAIN, K. E. The development of spatial resolving power of lateral geniculate neurones in kittens. *Exp. Brain Res.* 31: 193–206, 1978.

JONES, J. P. AND PALMER, L. A. The two-dimensional spatial structure of simple receptive fields in the cat striate cortex. *J. Neurophysiol.* 58: 1187–1211, 1987a.

JONES, J. P. AND PALMER, L. A. An evaluation of the two-dimensional Gabor filter model of simple receptive fields in cat striate cortex. *J. Neurophysiol.* 58: 1233–1258, 1987b.

KAUFMAN, D. A. AND PALMER, L. A. The luminance dependence of spatiotemporal response of cat striate cortical units (Abstract). *Invest. Ophthalmol. Visual Sci. Suppl.* 31: 398, 1990.

KULIKOWSKI, J. J. AND BISHOP, P. O. Linear analysis of the responses of simple cells in the cat visual cortex. *Exp. Brain Res.* 44: 386–400, 1981.

LENNIE, P. Parallel visual pathways: a review. *Vision Res.* 20: 561–594, 1980.

LEVICK, W. R. Another tungsten microelectrode. *Med. Biol. Eng.* 10: 510–515, 1972.

MAFFEI, L. AND FIORENTINI, A. The visual cortex as a spatial frequency analyzer. *Vision Res.* 13: 1255–1267, 1973.

MAFFEI, L., MORRONE, C., PIRCHIO, M., AND SANDINI, G. Responses of visual cortical cells to periodic and nonperiodic stimuli. *J. Physiol. Lond.* 296: 27–47, 1979.

MANGEL, S. C., WILSON, J. R., AND SHERMAN, S. M. Development of neuronal response properties in the cat dorsal lateral geniculate nucleus during monocular deprivation. *J. Neurophysiol.* 50: 240–264, 1983.

MARCELJA, S. Mathematical description of the responses of simple cortical cells. *J. Opt. Soc. Am.* 70: 1297–1300, 1980.

MARTIN, K. A. C. Neuronal circuits in cat striate cortex. In: *Cerebral Cortex,* edited by E. G. Jones and A. Peters. New York: Plenum, Vol. 2, p. 241–284, 1984.

MCLEAN, J. AND PALMER, L. A. Contribution of linear spatiotemporal receptive field structure to velocity selectivity of simple cells in the cat's striate cortex. *Vision Res.* 29: 675–679, 1989.

MITCHELL, D. E. AND TIMNEY, B. Postnatal development of function in the mammalian visual system. In: *Handbook of Physiology. The Nervous System. Sensory Processes.* Washington, DC: Am. Physiol. Soc. 1984, sect. 1, vol. III, p. 507–555.

MOORE, C. L., KALIL, R., AND RICHARDS, W. Development of myelination in optic tract of the cat. *J. Comp. Neurol.* 165: 125–136, 1976.

MOVSHON, J. A. The velocity tuning of single units in cat striate cortex. *J. Physiol. Lond.* 249: 445–468, 1975.

MOVSHON, J. A., THOMPSON, I. D., AND TOLHURST, D. J. Spatial summation in the receptive fields of simple cells in the cat's striate cortex. *J. Physiol. Lond.* 283: 53–77, 1978a.

MOVSHON, J. A., THOMPSON, I. D., AND TOLHURST, D. J. Receptive field organization of complex cells in the cat's striate cortex. *J. Physiol. Lond.* 283: 79–99, 1978b.

MOVSHON, J. A., THOMPSON, I. D., AND TOLHURST, D. J. Spatial and temporal contrast sensitivity of neurones in areas 17 and 18 of the cat's visual cortex. *J. Physiol. Lond.* 283: 101–120, 1978c.

MOVSHON, J. A. AND VAN SLUYTERS, R. C. Visual neural development. *Annu. Rev. Psychol.* 32: 477–522, 1981.

OHZAWA, I., DeANGELIS, G. C., AND FREEMAN, R. D. Stereoscopic depth discrimination in the visual cortex: neurons ideally suited as disparity detectors. *Science Wash. DC* 249: 1037–1041, 1990.

OHZAWA, I. AND FREEMAN, R. D. The binocular organization of simple cells in the cat's visual cortex. *J. Neurophysiol.* 56: 221–242, 1986.

ORBAN, G. A. Quantitative electrophysiology of visual cortical neurones. In: *Vision and Visual Dysfunction. The Neural Basis of Visual Function,* edited by A. G. Leventhal. Boca Raton, FL: CRC, 1991, vol. 4, p. 173–222.

PALMER, L. A. AND DAVIS, T. L. Receptive-field structure in cat striate cortex. *J. Neurophysiol.* 46: 260–276, 1981.

PALMER, L. A., JONES, J. P., AND STEPNOSKI, R. A. Striate receptive fields as linear filters: characterization in two dimensions of space. In: *Vision and Visual Dysfunction. The Neural Basis of Visual Function,* edited by A. G. Leventhal. Boca Raton, FL: CRC, 1991, vol. 4, p. 246–265.

PASTERNAK, T. AND MERIGAN, W. H. The luminance dependence of spatial vision in the cat. *Vision Res.* 21: 1333–1339, 1981.

PETTIGREW, J. D. The effect of visual experience on the development of stimulus specificity by kitten cortical neurones. *J. Physiol. Lond.* 237: 49–74, 1974.

REID, R. C., SOODAK, R. E., AND SHAPLEY, R. M. Linear mechanisms of directional selectivity in simple cells of cat striate cortex. *Proc. Natl. Acad. Sci. USA* 84: 8740–8744, 1987.

REID, R. C., SOODAK, R. E., AND SHAPLEY, R. M. Directional selectivity and spatiotemporal structure of receptive fields of simple cells in cat striate cortex. *J. Neurophysiol.* 66: 505–529, 1991.

RUSOFF, A. C. AND DUBIN, M. W. Development of receptive-field properties of retinal ganglion cells in kittens. *J. Neurophysiol.* 40: 1188–1198, 1977.

SAUL, A. B. AND HUMPHREY, A. L. Temporal-frequency tuning of direction selectivity in cat visual cortex. *Visual Neurosci.* 8: 365–372, 1992.

SHERK, H. AND STRYKER, M. P. Quantitative study of cortical orientation selectivity in visually inexperienced kitten. *J. Neurophysiol.* 39: 63–70, 1976.

SKOTTUN, B. C., DeVALOIS, R. L., GROSOF, D. H., MOVSHON, J. A., ALBRECHT, D. G., AND BONDS, A. B. Classifying simple and complex cells on the basis of response modulation. *Vision Res.* 31: 1079–1086, 1991.

STORK, D. G. AND WILSON, H. R. Do Gabor functions provide appropriate descriptions of visual cortical receptive fields? *J. Opt. Soc. Am. A* 7: 1362–1373, 1990.

SUTTER, E. E. A revised conception of visual receptive fields based upon pseudorandom spatiotemporal pattern stimuli. In: *Proceedings of First Symposium on Testing and Identification of Nonlinear Systems.* Pasadena, CA: California Institute of Technology, 1975, p. 353–365.

SZULBORSKI, R. G. AND PALMER, L. A. The two-dimensional spatial struc-

ture of nonlinear subunits in the receptive fields of complex cells. *Vision Res.* 30: 249–254, 1990.

SZULBORSKI, R. G. AND PALMER, L. A. Linear behavior of complex cell subunits in cat striate cortex (Abstract). *Invest. Ophthalmol. Visual Sci. Suppl.* 32: 1253, 1991.

TADMOR, Y. AND TOLHURST, D. J. The effect of threshold on the relationship between the receptive-field profile and the spatial frequency tuning curve in simple cells of the cat's striate cortex. *Visual Neurosci.* 3: 445–454, 1989.

TOLHURST, D. J. AND DEAN, A. F. Evaluation of a linear model of directional selectivity in simple cells of the cat's striate cortex. *Visual Neurosci.* 6: 421–428, 1991.

TSUMOTO, T. AND SUDA, K. Laminar differences in development of afferent innervation to striate cortex neurons in kittens. *Exp. Brain Res.* 45: 433–446, 1982.

WATSON, A. B. AND AHUMADA, A. J. A look at motion in the frequency domain. *NASA Tech. Memo.* 84352: 1–10, 1983.

WATSON, A. B. AND AHUMADA, A. J. Models of human visual-motion sensing. *J. Opt. Soc. Am. A* 2: 322–342, 1985.

WIENER, N. *Nonlinear Problems in Random Theory.* New York: Wiley, 1958.

ZUMBROICH, T., PRICE, D. J., AND BLAKEMORE, C. Development of spatial and temporal selectivity in the suprasylvian visual cortex of the cat. *J. Neurosci.* 8: 2713–2728, 1988.